University of Thessaly
School of Engineering
Department of Mechanical Engineering

Thesis

Influence of stepped repair parameters on the mechanical performance of wind turbine blade's outer shell

by

DRIVAS THEMISTOKLIS
University of Thessaly, 2020

Submitted in Partial Fulfilment of
the Requirements for the Degree of Master of Science
2020

Approved by the Three Members of the Advisory Committee:

First Member (Supervisor)
ALEXIS KERMANIDIS
Associate Professor
Department of Mechanical Engineering, University of Thessaly

Second Member
SPYROS A. KARAMANOS
Professor
Department of Mechanical Engineering, University of Thessaly

Third Member
MICHALIS AGORAS
Assistant Professor
Department of Mechanical Engineering, University of Thessaly

Acknowledgements

First of all, I would like to thank my supervisor, Associate Professor Alexis Kermanidis, for his valuable help and guidance during my master of science thesis and for the knowledge I gained from his teaching, in related lessons in the field of materials science. I am also grateful to the members of my examination committee, my professor Alexis Kermanidis as well as the professor Spyros A. Karamanos and Michalis Agoras for their valuable suggestions and for the knowledge they have given me both in the context of this thesis and throughout my undergraduate studies in the department of mechanical engineering. I would also like to thank the Ph.D. candidate Christos Prosgolitis for his assistance in the experiments carried out at the Laboratory of Materials, during the preparation of this thesis on theoretical issues arising from the data processing. Finally, i have to thank my parents and my friends for their support throughout all these studying years, so I will dedicate this study to them.

Table of Contents

List of figures

List of tables

Summary

Wind turbine blades are subjected to cyclic alternating mechanical loads and the conditions under which they operate are often unfavorable because of the locations they are usually installed are mountain peaks or offshore. This, in combination with the fact that wind turbines have a continuous service life of 20 to 25 years, means that they are vulnerable to potential structural damage which, if left untreated, can lead to total blade destruction. This is why it is often necessary to have the blades repaired immediately by specialized technicians who carry out the repairs, in accordance with the blades manufacturer's instructions, without the need to detach the blade from the wind turbine. Applied repair procedures may vary in type and should provide similar mechanical characteristics to the virgin material.

In the present study an attempt is made to determine the characteristics influencing the mechanical durability of the stepped repair procedure in composite fiber reinforced materials by which the wind turbine blades are constructed. In particular, the bending and tensile behavior of repaired structural component of wind turbine blades is studied in accordance with the length of the overlap used in the procedure. During the experimental procedure, four-point bending and tensile specimens were constructed in accordance with international standards, which were then subjected to the respective tests.

The conclusions from this experimental study are useful as they can be used as a guide for selecting the right overlap length in a repair and understand better all the repair factors. Finally, the present study provides a better understanding of the bending behavior of the section including the repair and its failure characteristics.

1. INTRODUCTION

1.1 General

The search for renewable energies in recent decades has become more and more intense as energy production is unlimited and “cleaner” than fossil fuels. Moreover, the evolution of the wind turbine industry has been rapid, as the hub height and the blade’s length as well as the maximum power output are constantly increasing, which makes the wind turbine generators an attractive option for the generation of electricity.

One of the main components of the wind turbines is the blade, which comes in contact with the wind and is "responsible" for converting the wind energy into a rotary motion of a rotor thus electrical energy. The overall surface area, the shape as well as the weight of the blades play a crucial role in the overall performance of a wind turbine and the energy outcome.

The most common materials from which the modern wind turbine blades are made from are fiber reinforced polymeric materials, i.e. a combination of carbon fiber, fiberglass, core material, epoxy resin system. The combination of these materials in a specific way can lead to the construction of a blade with a very large surface, light weight and great stiffness.

Wind turbines are mainly located in places with a high speed and smooth wind flow. In particular, these machines are placed either in terrain areas such as ridges or offshore. This means that the weather and environmental conditions under which wind turbines operate, and hence the blades, are usually unfavorable. A fact that, combined with continuous movement and the constant cyclic loads often leads to intense damage of the blades.

Therefore, in order to ensure a satisfactory and uninterrupted operation of at least 20 years, there is always an urgent need for preventive checks in order to identify any problems in a timely manner and to conduct a repair in accordance with the manufacturer's instructions. By this method it is possible, to avoid the progression of damages which can lead to complete destruction of the blades.

The number of the case studies, that have dealt with repair methods in E-glass fiber reinforced plastic materials and parameters that affect either positive or negative the durability of the repairs to various mechanical loads, is limited. Motivated by the work of Zonghong Xie, Xiang Li and Qun Yan [1], who studied factors that influence scarf repair on carbon-fiber composite laminates in the present study, a stepped repair study is carried out on E-glass fiber-reinforced composite materials.

1.2 Purpose of the thesis

In the present study, the influence of stepped repair parameters on the strength of Glass Fiber Reinforced Composite Materials are investigated. The main reason for choosing these materials is their widespread use in many modern constructions, since they have very good mechanical properties in relation to their weight, for example such materials are usually found in wind turbine blades. In particular, the type of repair being studied is the "stepped repair" according to the study by C. H. Wang, V. Venugopal and L. Peng [2].

2. BIBLIOGRAPHICAL REVIEW

2.1 Historical overview

At the end of the 20th century, the oil crisis happened as well as the intense climate change that arose from the unprecedented anthropogenic environmental burden on the planet (industrial orgasm). These events have prompted the science and research community to speed up the development of renewable sources of renewable electricity as an alternative to burning fossil fuels as they are abundant, renewable, widely distributed, don't produce greenhouse gas emissions and do not burden the environment, fact that is demanded by modern societies. All the above, lead to a rapid growth in the technological development of wind turbines. In particular, in 1887 Charles F. Brush completed the construction of the first 12 kW wind turbine generator, 18 meters tall and weighing 4 tons, shown in Figure 1. This construction is aimed at an energy-independent home [3].

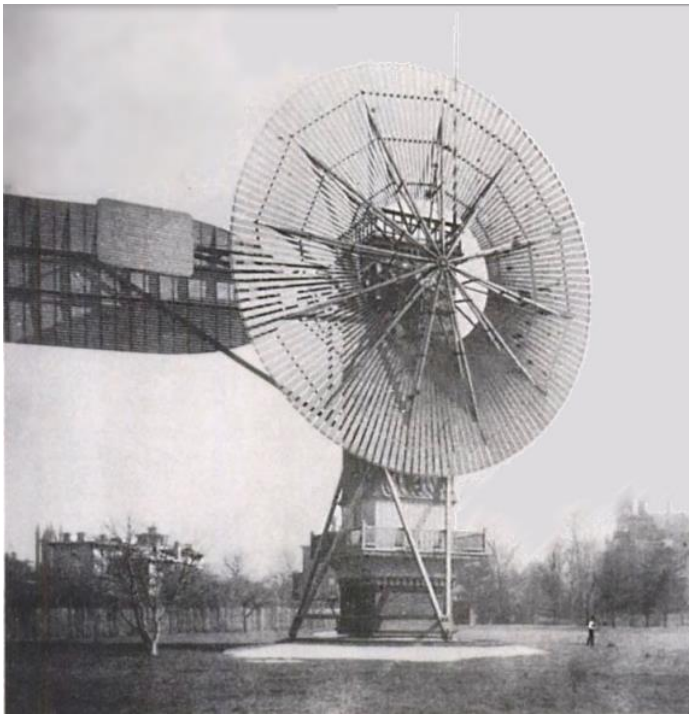

Figure 1 – Image – Charles F. Brush wind generator

Since then, there has been a continuous attempt to improve the efficiency and therefore to increase the produced energy outcome on how wind turbines will have the highest possible performance and operational lifetime. Thus, over time, wind turbines are gaining an ever-increasing height as well as an ever-increasing rotor diameter in order to increase energy output and optimize efficiency, as shown in Figure 2. However, this optimization is limited by the strengths of the materials used, thus highlighting the importance and necessity of the evolution of material science.

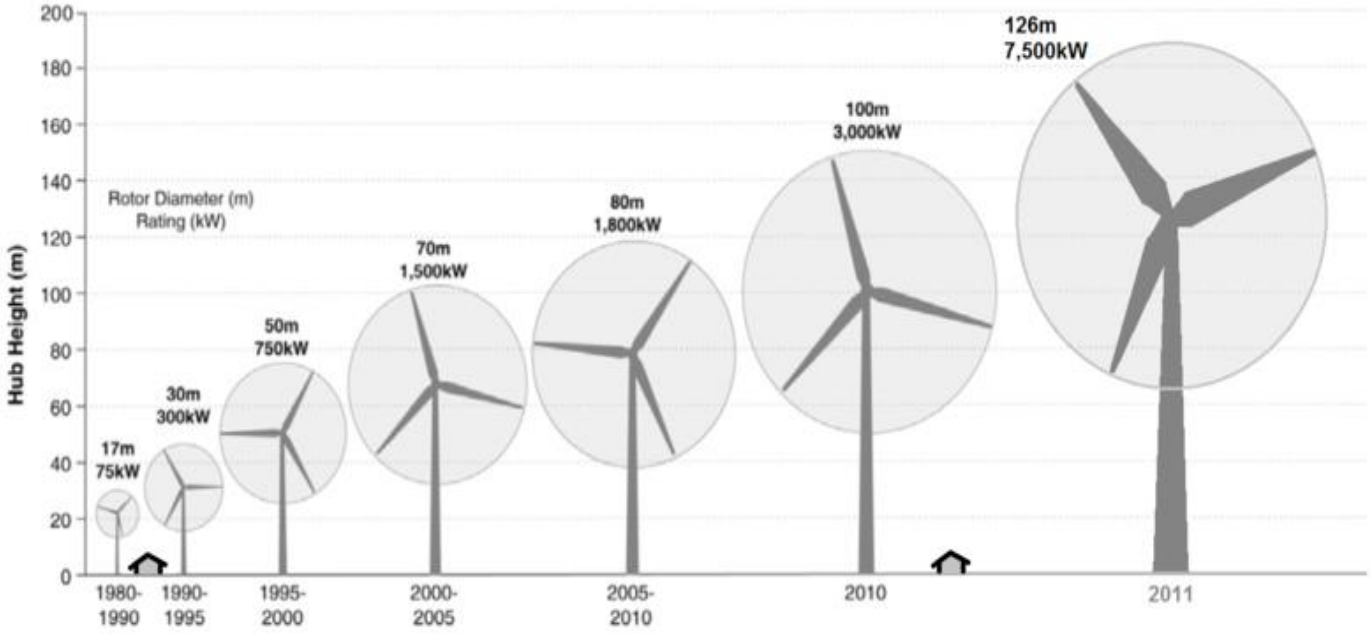

Figure 2 – Image – Diagram of the wind turbine development over time

2.2 Structure of blades

The blade design begins with a basic compromise between aerodynamic shape and structural integrity. The choice of materials and manufacturing process affects how thin and aerodynamic blades can be manufactured and the final cost. Therefore, material science plays a crucial role in bringing together the design and production industries together to find the best solution for performance and cost.

Nowadays almost all blade manufacturers conclude to almost the same and simple blade design. The particular blade structure (Figure 3), which is predominantly common, consists of two main parts [4].

1) The **central spar beam** that gets loaded from gravitational, centrifugal and mainly aerodynamic forces, ie the bending of the blade due to pressure-lift side. Spar is also the one that attaches itself to the rotor and is therefore the "root" of the wing

2) However, the blade must have an aerodynamic shape, so the Spar is enclosed by an **aerodynamic shell** whose cross-section is designed to create diverging fluid flow velocities and various pressures which then result in rotary movement of the rotor.

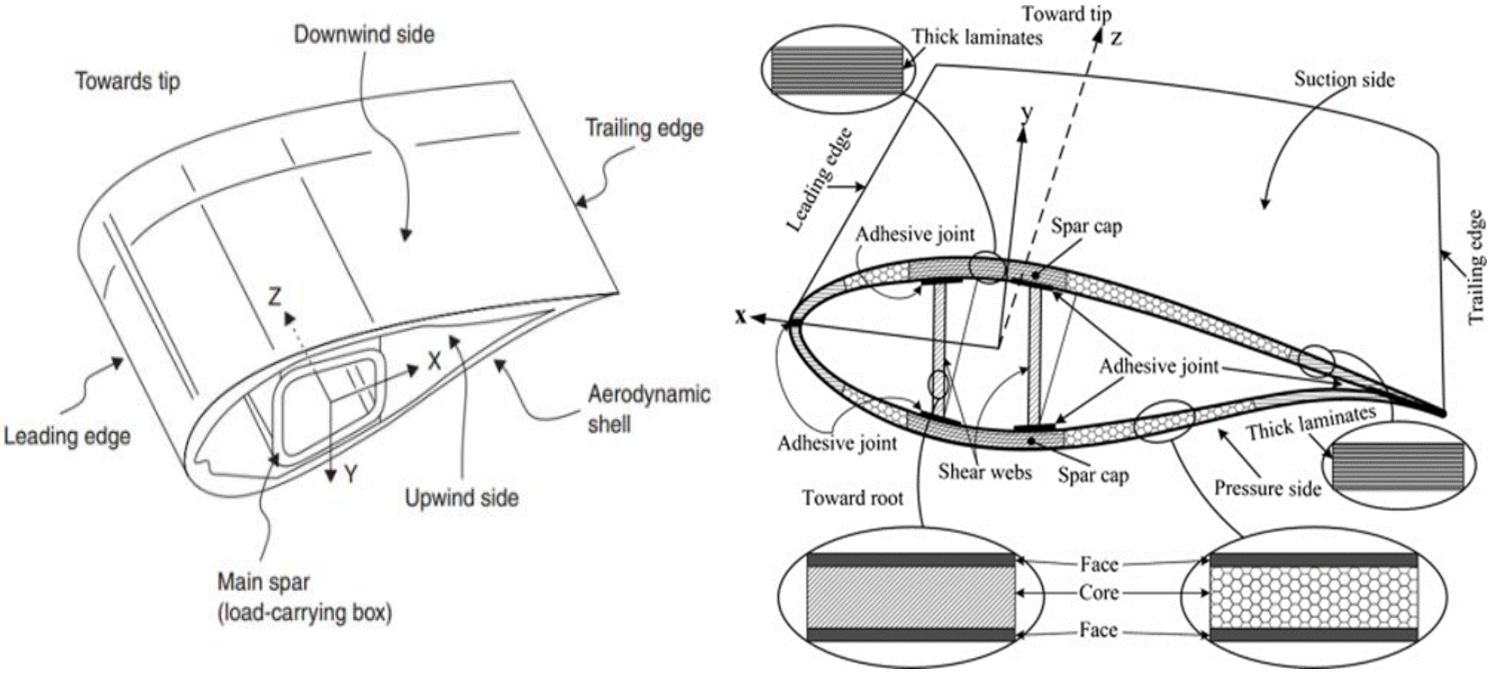

Figure 3 – Image – Morphology of a wind turbine blade

Modern wind turbine blades are made of Fiber Reinforced Plastic because of the better weight-to-durability ratio of the materials compared to the wood and metals previously used. These composite materials are particularly suited for long, thin structures such as blades, because most stresses are in one direction and the fibers can be aligned to fit. It is quite obvious that most of the fibers in the Spar as well as in the aerodynamic shell have to be oriented along the length of the blade as it is the direction of the bending loads, tension on windward side and compression on the leeward side.

2.3 Structural damages in wind turbine blades

Wind turbine blades are often subjected to complex loads under demanding operating conditions like extreme temperatures, high humidity, corrosion, lightning strikes, bird strikes. As wind turbines are evolving and their size are constantly increasing, their operating loads also increase significantly (e.g., the blade weight increases significantly with increasing the length, thus increasing gravity and inertial loads). In addition, for offshore installations, service conditions differ significantly from those of land-based installations. A blade is typically subjected to flat-wise and edge-wise bending as shown in Figure 4 [5], gravity loads (generally produce edge-wise bending), torsional loads, axial load due to rotation of the blade (inertia forces) and loads due to decelerations and accelerations [4].All of the above, factors often lead to some common damages of the blades like these shown in Figure 5.

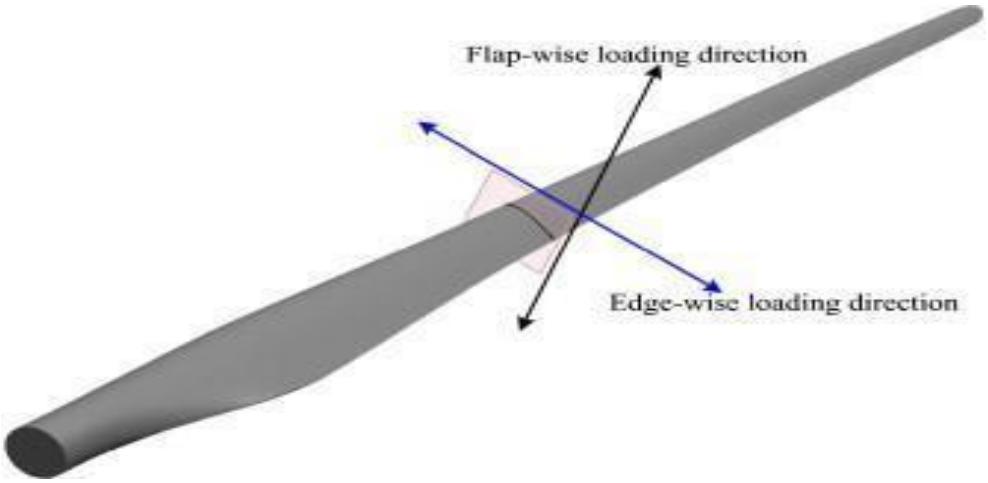

Figure 4 – Image – Basic loading directions of a wind turbine blade

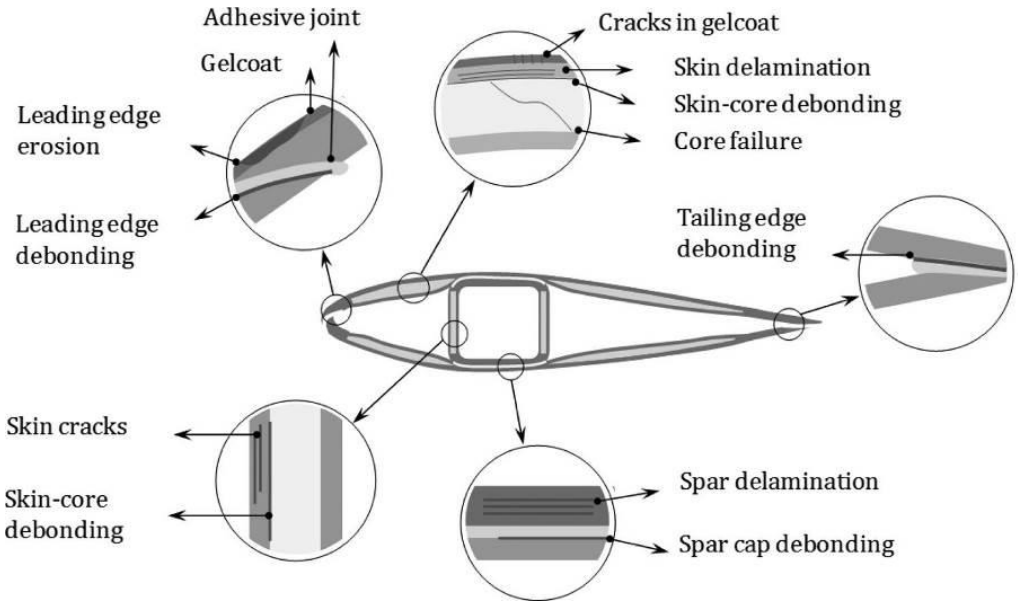

Figure 5 – Image – Common damages in wind turbine blades

2.4 Materials and properties

The most popular materials used in modern wind turbine blades are laminated composites consisting of laminated fabrics (glass-fiber fabrics, carbon-fiber fabrics) in combination with core material like polyurethane foam, the placement of the materials is shown in Figure 6. The impregnation of these fabrics with various kinds of resins (epoxy systems) leads to the formation of fiber reinforced plastics. The different placement sequence and the different knitting fabrics create many different combinations of materials with different mechanical properties. Therefore, depending on the part and the area of the blade different combinations of laminate sandwich are used [6].

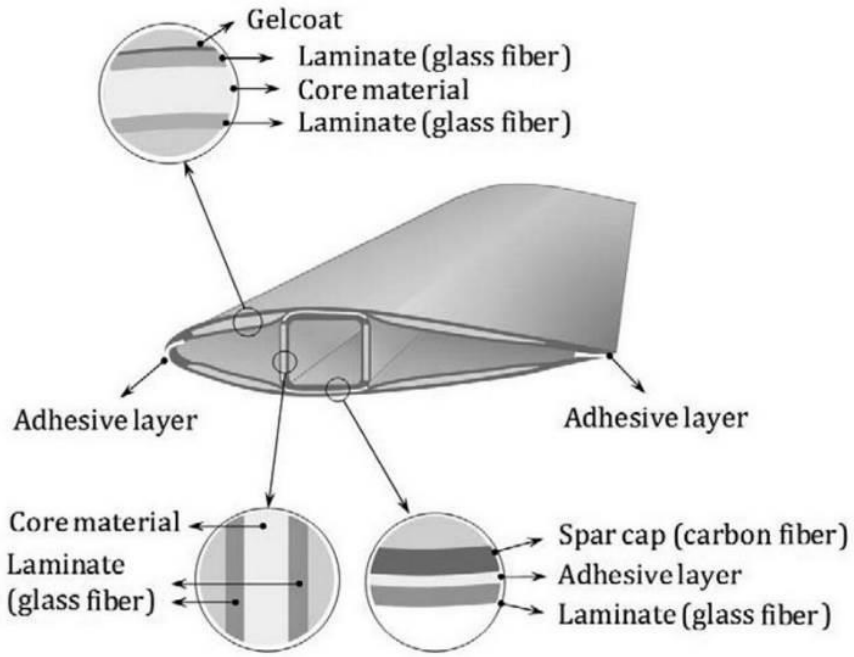

Figure 6 – Image – Materials used over the blade's cross section

Composite materials nowadays are found in numerous applications as they exhibit some excellent properties in comparison to conventional structural materials. Light weight, high strength, excellent corrosion resistance, very good fatigue, impact and crack propagation resistance, relatively easy manufacturing processes and low maintenance costs are some of the factors contributing to the deployment of composite materials. Disadvantages of composite materials are high creep levels, low resistance to mechanical deterioration, particular and often sensitive behavior in adverse environmental conditions (marine environment, extremely high-low temperatures, chemical environment) and their fairly high initial cost. These problems are gradually and effectively addressed through continued technological development in the design and production industries of new methods and better types fibers and resins.

2.4.1 Types of fibers

The "fiber-fabrics" that make up the polymer composites found on the blades are essentially stitches of glass or carbon fibers. Carbon fibers exhibit very high strengths as well as great stiffness, helping the surrounding resin to withstand fatigue by reducing the resin load. It is well known, that carbon fibers are much more costly, therefore they tend to be used only where their properties are necessary, for example in the spar beam of the blade. In large modern blades, reaching up to 88.4m, carbon fibers are necessary, as in such big blades it is much harder to achieve sufficient rigidity without adding too much weight. Thus, the most common combination of materials is carbon fibers in the main structural element of the blades, namely the spar beam which receives and the main loads, while in the outer aerodynamic shell glass fibers are used. Finally, depending on how many bundles of fibers are knitted, many combinations and categories of fabrics are created.

The key benefits of **glass fiber** (glass fiber fabrics) are low cost and high strength while their main drawbacks are the low modulus of elasticity and low strength against friction wear. Surface engravings and scratches also create stress concentration regions, resulting in rapid deterioration of their mechanical properties and their adhesion to the polymer matrix.

Carbon fiber is one of the most predominant reinforcement, because of their high strength and high elastic modulus. The combination of carbon fiber and resin matrix is used to produce high performance composite materials such as the spar beam which is the main structural element of the blade. In general, where the optimal combination of mechanical behavior and weight reduction is required, the fibers used are usually carbon fibers. Also, carbon fibers are preferred when the thermal expansion of a material has to be low or when compatibility of the expansion characteristics of two combined different materials is required. This carbon propensity is due to the nature of the carbon and the intrinsic bonds it forms with other carbon atoms. graphite consists of anisotropic polycrystallins, whose anisotropy depends on their manufacturing conditions [7].

2.4.2 Forms of fiber-fabrics

Fibrous composites are distinguished according to the orientation and layout of the fibers within the matrix. According to this classification the fibrous composites are distinguished in:

- Unidirectional composites, in which all the fibers have the same direction.
- Multi-directional composites, in which, the fibers have different directions.

Multi-directional fabrics are classified into the following subgroups:

- Composite with random-source fibers.
- Composites with weave fibers.

There are many types of knitting that are mainly categorized by the number of knits, as well as by the directions of the fibers (unidirectional, biaxial, triaxial). An additional distinction of fibrous composites is based on the ratio of length to diameter $\frac{l}{d}$ of the fibers, which are characterized as:

- Continuous or long fibers, when it is $\frac{l}{d} \geq 100$
- Discontinuous or discontinuous fibers, when it is $\frac{l}{d} \leq 100$
- Threads or whiskers: With d <1μm and $l \cong 100\mu m$

Also, another basic feature of glass fiber is its density g/m^2, as the higher the density, the more fibers and hence the higher the strength.

In the present study we use the following fiberglass fabrics:

- Biaxial 310gr/m^2
- Triaxial 1185gr/m^2

2.4.3 Core material

Engineering theory shows that the flexural stiffness of any beam is proportional to its cube of thickness. The purpose of a core material in a composite laminate is therefore to increase the stiffness of the laminate by effectively "thickening" it with a low-density core material. This can provide a dramatic increase in stiffness with a very small extra weight. In modern wind turbines, mainly foamed materials derived from the family of PVC plastic (polyvinyl chloride) is used.

The idea of using relatively thin, strong fibrous sheets bonded with thicker core materials has allowed the industry to build strong, stiff, lightweight and extremely durable structures that would otherwise not be practical. The core materials are very light in shape and texture similar to hard sponge. Extruded polyurethane consists of small closed cells that are impermeable to water or any other liquid. Therefore, with an increase in weight of only 3%, an increase in bending strength and stiffness by 3.5 times and 7 times respectively can be achieved if the core material has been properly combined with fibrous polymers. Thus, resulting to the final multilayer composition of the foamed glass materials results.

2.4.4 Matrix material

The matrix material is perhaps the most important material in fibrous composites as it serves two very important functions. On the one hand, it maintains the fibrous phase in its place, enclosing it, on the other hand under the application of high forces it deforms and distributes the tension to the high modulus of elasticity component, the fibers. Equally important roles of the matrix material are the protection of the fibers from environmental damage and corrosion insults as well as the inhibition of the propagation of cracks that start from breakage of fibers. The matrix materials are selected on the basis of the desired properties, in particular in the wind turbine blade industry, thermosetting resins (epoxy, polyester) are used. The reason for this choice is the ease of wetting of the low viscosity resin reinforcing agent systems, at the blade production stage and the phenomenal mechanical properties of these systems (especially epoxy systems).

In order to satisfy its roll, a loaded matrix material must be characterized by ductility, durability, relative rigidity. Moreover, the melting point of the matrix material have to be much greater than the maximum operating temperature of the composite. These properties must also be "compatible" with the corresponding properties of the reinforcing fibers. Typically, the matrix material has a lower density, stiffness and fatigue durability than fibers. Last but not least in order to achieve good characteristics and a proper operation of the composite material, really important factor is the good fiber-matrix adhesion, i.e. good impregnation during the manufacture of the composite material.

3. EXPERIMENTAL PROCEDURE

3.1 Objective

The experimental investigation is carried out by using specimens made of composite materials with exactly the same sequence that the most of aerodynamic blade shell are made. In the experimental procedure the stepped repair technique has been implemented and the influence of parameters such as the size (overlap) and number of steps used in the repair on the composite structure mechanical performance have been assessed. The mechanical performance of the composite blade structure has been evaluated under static axial and bending loads.

Specifically:

- Determination of flexural strength as well as determination of flexural properties in four-point bend specimens according to ASTM 7264 / D 7264-M [8].
- Determination of tensile strength in tensile test pieces according to ASTM D 3039/D 3039M [9].

have been performed.

3.2 Specimen materials

In the present study, biaxial, triaxial fiber-fabrics in combination with epoxy thermosetting resin are used, as well as polyvinyl chloride foam is used as core material in the center of the lamination. The supply of materials was made by FIBERMAX COMPOSITES © as well as by ALPHAKEM ©

Technical characteristics of the materials used:

1. Biaxial fiberglass: 2 fiber directions (+, - 45^o), weight 310 g /m^2 (Figure 7)

2. Triaxial fiberglass: 3 fiber directions (+, - 45^o, 0-90^o), weight 1185 g /m^2 (Figures 8,9)

3. Epoxy resin: FIBERMAX R481 with hardener H17, weight ratio 18/100

4. Core material 80/30 (PVC foam): Thickness 30mm

Figure 7– Image – Biaxial fiberglass fabric

Figure 8– Image – The unidirectional side of a triaxial fiberglass fabric

Figure 9– Image – The biaxial side of a triaxial fiberglass fabric

3.3 Preparation and structure of the specimens

3.3.1 Preparation of the specimens

Preparing the specimens is a complicated process similar to that followed by the blade makers for the construction of the outer shell. Initially, a smooth surface is moistened with a release agent material, after which the construction of the specimen begins and the lay-up of the fiber glass fabrics takes place. The lay-up sequence of the glass fiber fabrics and core material used, were the same with the actual structure are found on the outer shell of the blades. Specifically, the lay-up sequence depends on the type of specimen produced. After the impregnation of the glass fiber fabrics and the core material with the matrix material (epoxy system) is completed, then the vacuum process is followed in order to achieve perfect adhesion between the layers and to eliminate the excess material which adds excess weight to the structure. During vacuum procedure, the thermosetting matrix material must be solidified, for this reason the vacuum membrane is sealed, heat is supplied to the specimen using special lamps and blankets (in the industry special ovens are used). The procedure followed for the manufacturing of the specimens is shown schematically in Figures 10,11.

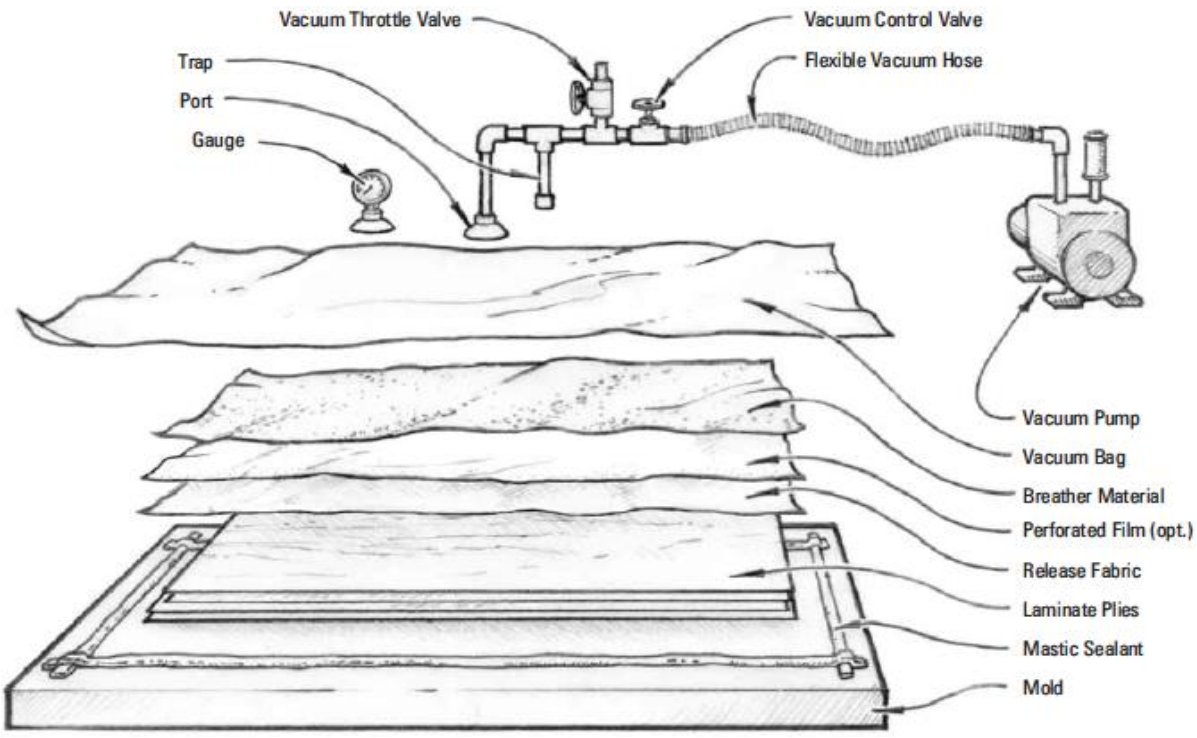

Figure 10 – Image – Vacuum Procedure

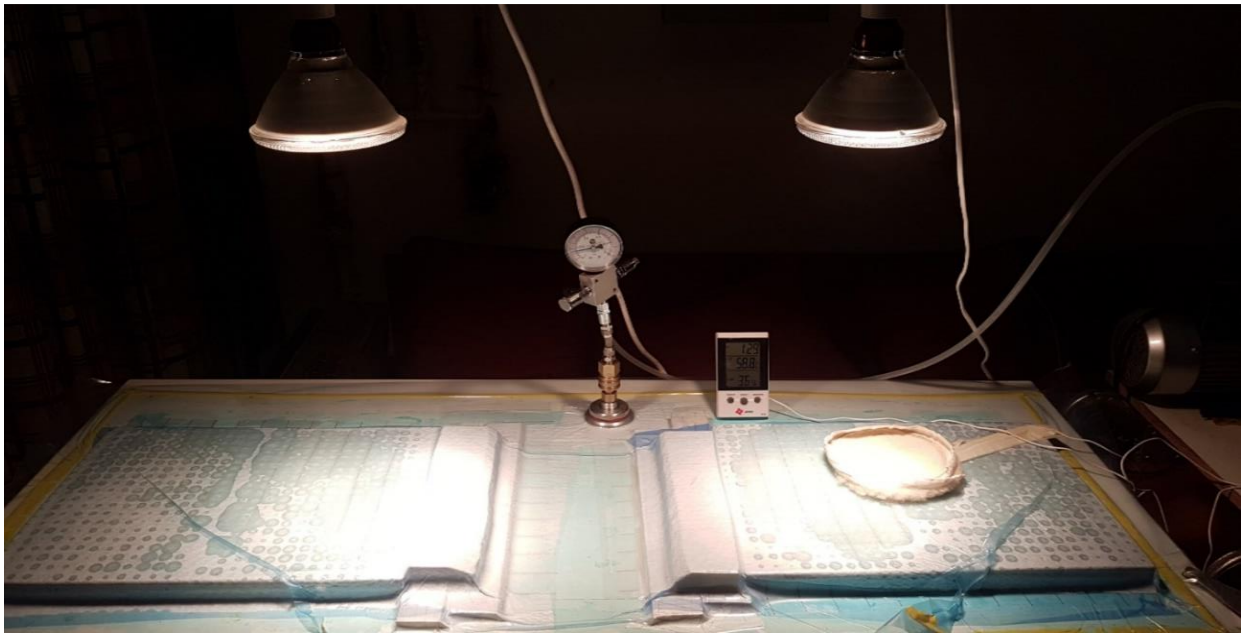

Figure 11 – Image – Ongoing vacuum-curing procedure after the impregnation of the fiberglass fabrics

In test specimens with no repair, the above procedure is followed only once, and in the case of the specimens with stepped overlap repair, the procedure is followed twice. In the case of a repair, the base with ready-made stairs is first constructed, when solidified, the base steps are scrubbed with grit 80 sand wheel in order to achieve proper adhesion between the added fiberglass fabrics of the repair and the base. Upon completion of the base preparation shown in Figures 11,12 the second phase of the construction starts, where in essence the steps prepared to receive the repair fiberglass fabrics so the final structure is formed.

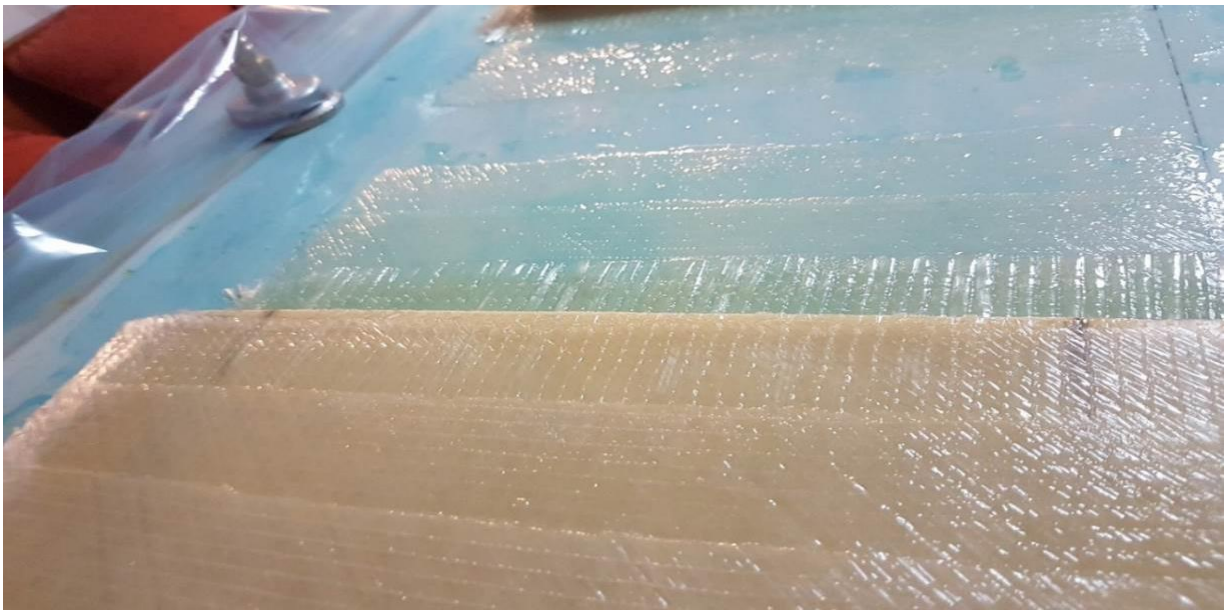

Figure 12 – Image – The fiberglass fabrics are impregnated in a step orientation in order to form a stepped base

3.3.2 Bending specimens

The bending specimens have the structure of the aerodynamic blade's shell as the layered layout of the structure is three glass fabrics on either side of the polyurethane foam (core material). The specimens are divided into two main categories, the reference specimens lacking a 'repair' in their structure and the specimens with stepped overlap repair in their structure with different step lengths. The bending specimens were designed in accordance with **ASTM 7264 / D 7264-M.**

Four different types of specimens were used in the experiment and 2 tests were performed for each category. In particular, the test categories are:

1. no repair
2. stepped repair overlap 20mm
3. stepped repair overlap 30mm
4. stepped repair overlap 40mm

The dimensions of the specimens used are shown in the Table 1 below:

BENDING SPECIMEN DIMENSIONS	
Width	120mm
Length	1000mm
thickness	40mm

Table 1 – Basic dimensions of the specimens

The specimen lamination and structure in this series of specimens is as follows (Figures 13,14):

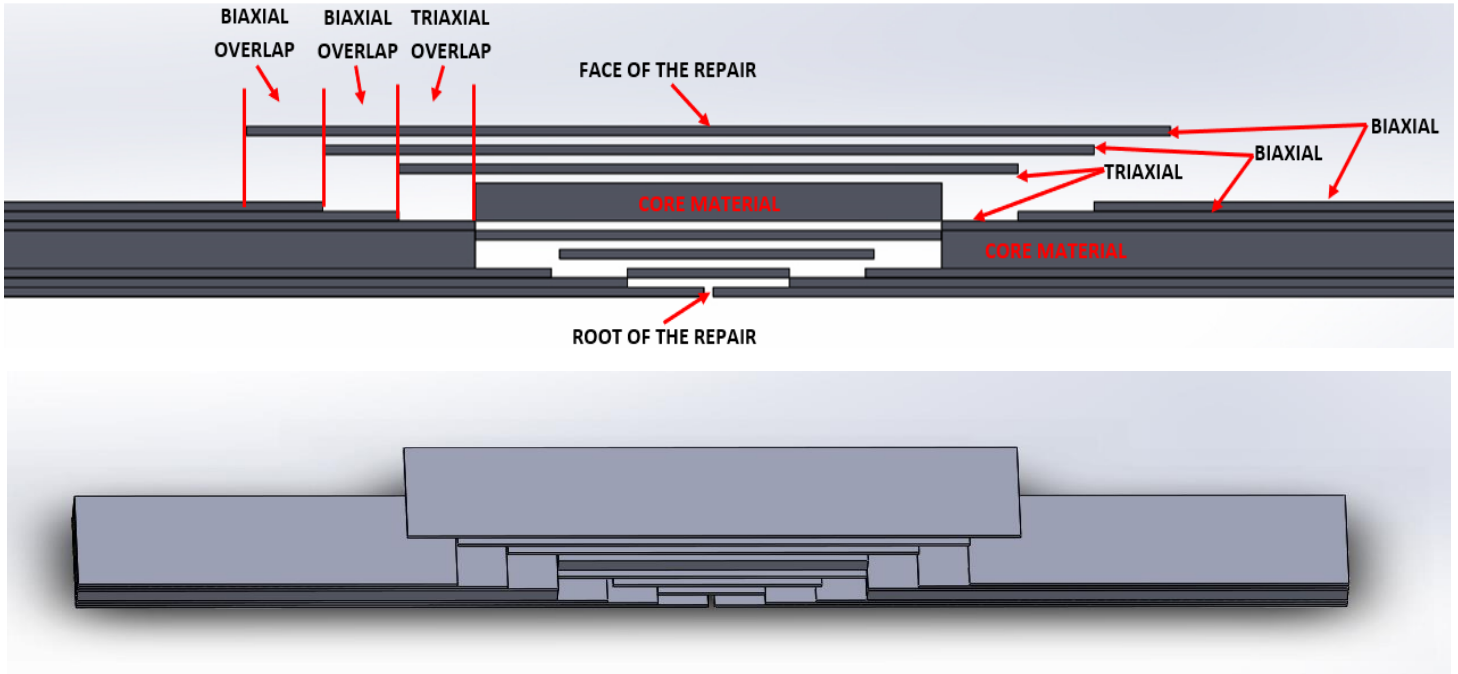

Figure 13 – Image – Model of the lamination of a bending specimen with a stepped repair

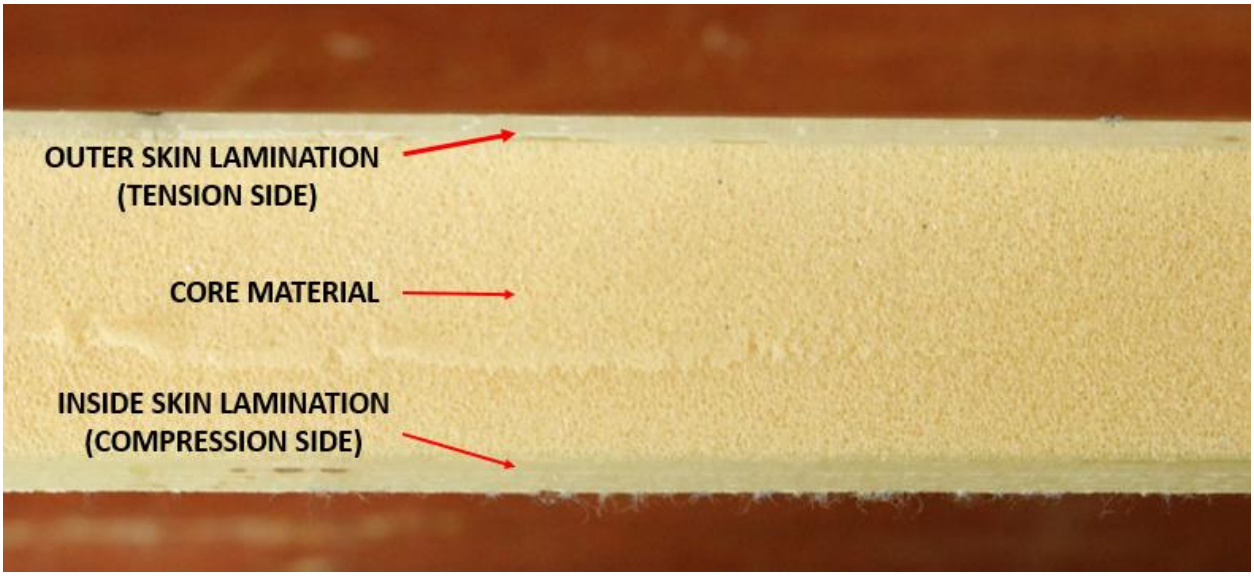

Figure 14– Image – The lamination of a bending specimen with a stepped repair

3.3.3 Tensile Specimens

The tensile specimens have the structure only of the outer laminate of the blade's shell. This means that the tensile specimens are made only from a three-fiber fabric lamination, which consists of one triaxial and two biaxial fabrics. The main categories of these specimens are the specimens with no repair in their structure and the specimens that have a repair in their structure. The repaired specimens are divided in three main categories depending on the length of the stepped overlap. In the tensile specimens, end tabs have been used in order to avoid failure to the gripping location during the tensile experiments (Figure 16). The tensile specimens were designed in accordance with **ASTM D 3039 / D 3039M**. Two different main test categories (no repaired, repair) and five tests were performed for each class of specimens. More specifically, the categories are:

1. no repair
2. stepped repair with overlap 20mm
3. stepped repair with overlap 30mm
4. stepped repair with overlap 40mm

The dimensions of the specimens used are shown in the table 2 below:

TENSILE SPECIMEN DIMENSIONS	
Width	40mm
Length	500mm
Thickness	1.5-2.5mm (depending on the specimen)

Table 2 – Basic dimensions of the specimens

The specimen lamination in this series of specimens is as follows in Figure 15:

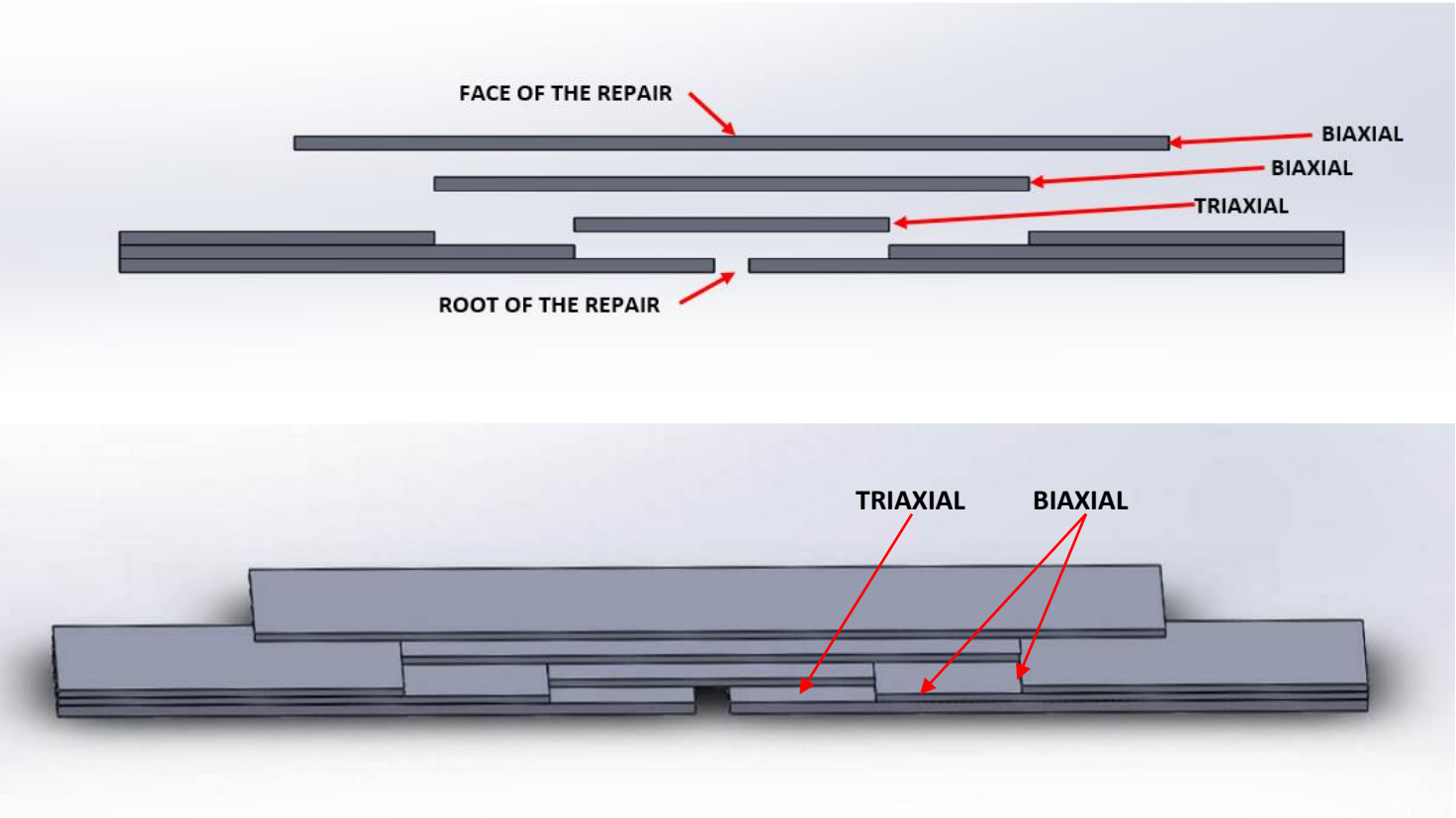

Figure 15 – Image – Model of the lamination of a tensile specimen with a stepped repair

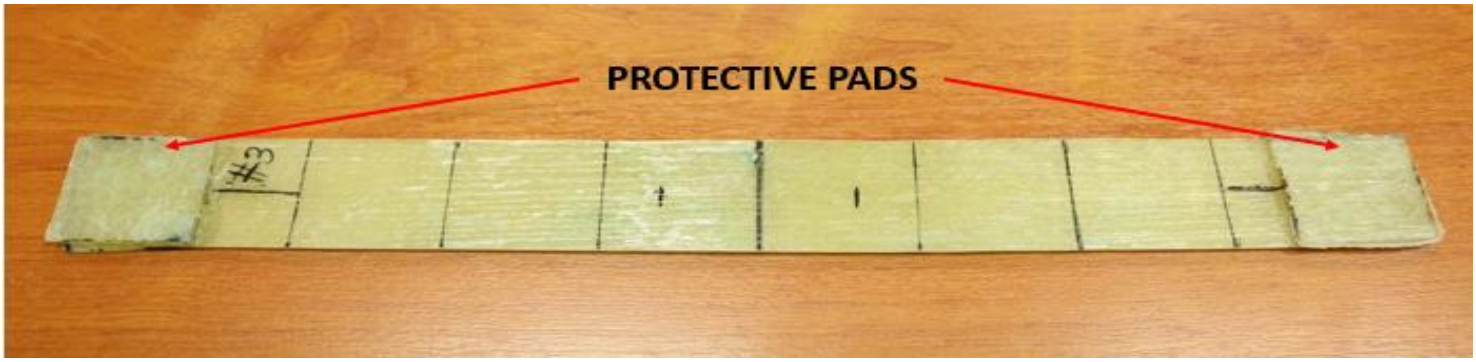

Figure 16 – Image – Tensile specimen with a stepped repair

3.4 Experimental setup

All the experiments were carried out at the Laboratory of Mechanics and Strength of Materials at the Department of Mechanical Engineering of the University of Thessaly and the tensile machine used is the Instron 8801. The tensile machine consists of three main parts, the high-pressure hydraulic system, the fixed loading frame in combination with the moving piston and the central controller console. All commands in the machine are given by PCs which are converted to different pressures through the console of the machine and through the closed loop circuit, to similar piston movements. At the top of the fixed frame there is the upper grapple, which has a load cell that essentially makes measurement of the load for each time of the experiment. The hole tensile machine setup is shown in Figure 17.

Figure 17 – Image – Tensile machine Instron 8801

3.4.1 Design and construction of a bending device

The main purpose of the experiments is to study the mechanical behavior of the composite structure including the stepped repairs carried out, the size of which was chosen to be on a full scale, like the actual repairs of the real structure. This demands the production of large-scale specimens which were manufactured in the frame of the present diploma thesis. In order to perform the bending experiments a special bending device shown in Figures 18,19 made of steel was constructed, capable of supporting specimens with long repair length. The four-point bending device used was a HEB 120 beam made of S355 structural steel. Taking into account the characteristics of the beam and the ASTM standard, the following device was developed in a way that can be adapted to different support openings according to the requirements of each experiment.

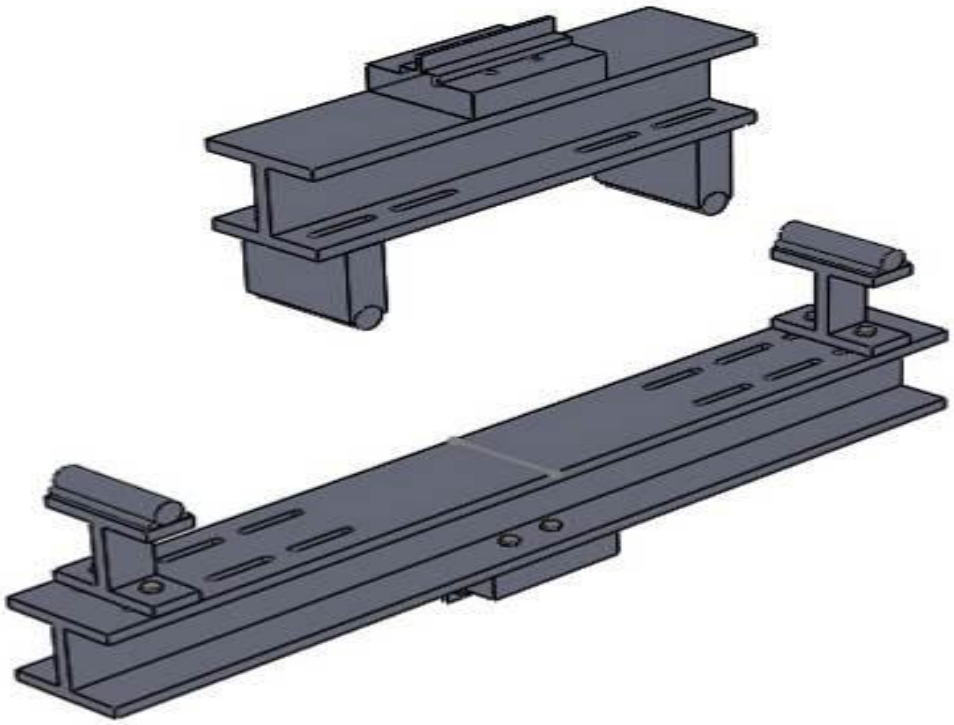

Figure 18 – Image – Four-point bending device

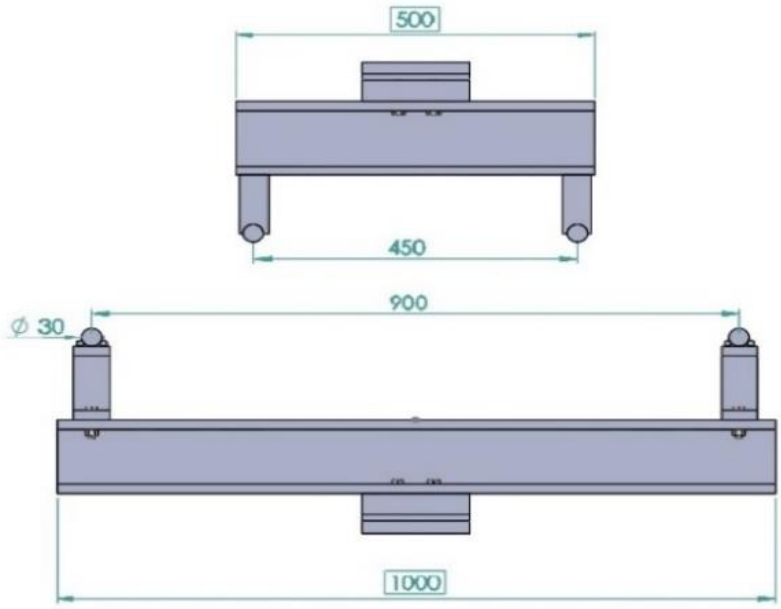

Figure 19 – Image – Dimensions (in mm) of the four-point bending device

In Table 3 the mechanical properties of the structural steel are given:

Yield Strength at nominal thickness 16mm	355 MPa
Tensile Strength at nominal thickness 16mm	630 MPa
Elongation at nominal thickness <40mm	22%
Brinel Hardness HB	146-187 HB
Density	7850 kg/m3

Table 3 – Properties of the four-point bending structural steel

3.5 Four-point bending experiment

Four-point static bending tests were performed at room temperature of 20 ° C with a constant extension rate of 1mm / min. During the experiment, displacement and load value were collected for the evaluation of the mechanical behavior. The four-point bending experimental setup is shown in Figure 20.

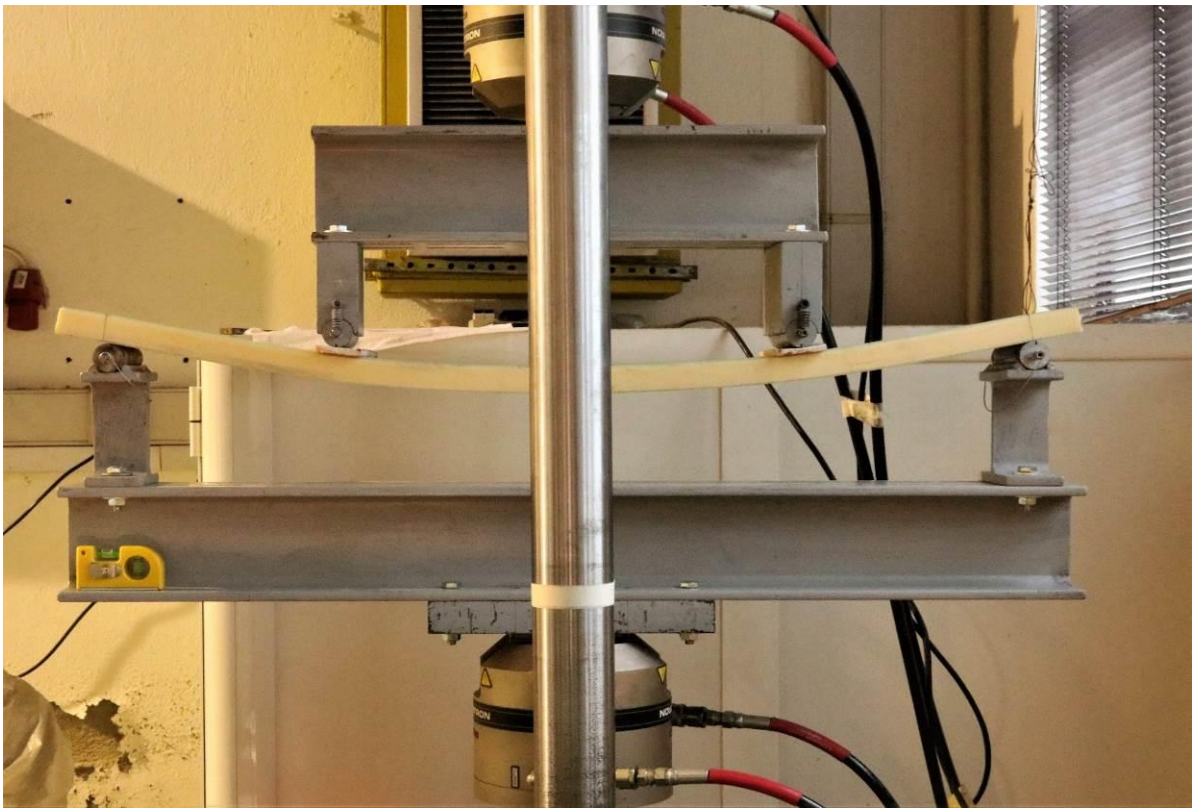

Figure 20 – Image – Four-point bending setup

For the calculations, the data obtained from load cell, displacement at the position of load application, the dimensions of each specimen as well as the bending support length have been used.

BENDING DEVICE DIMENSIONS	
Support span	900mm
Load span	450mm

Table 4 – Bending device dimensions

3.6 Tensile experiment

Static tensile tests were performed in accordance with ASTM D 3039 / D 3039M. The tests were carried out at a temperature of 20℃ and a displacement rate off 2mm / min. During the experiment, the data collected were load and displacement, as well as strain using an axial extensometer placed on the specimen's gauge length (Figure 21).

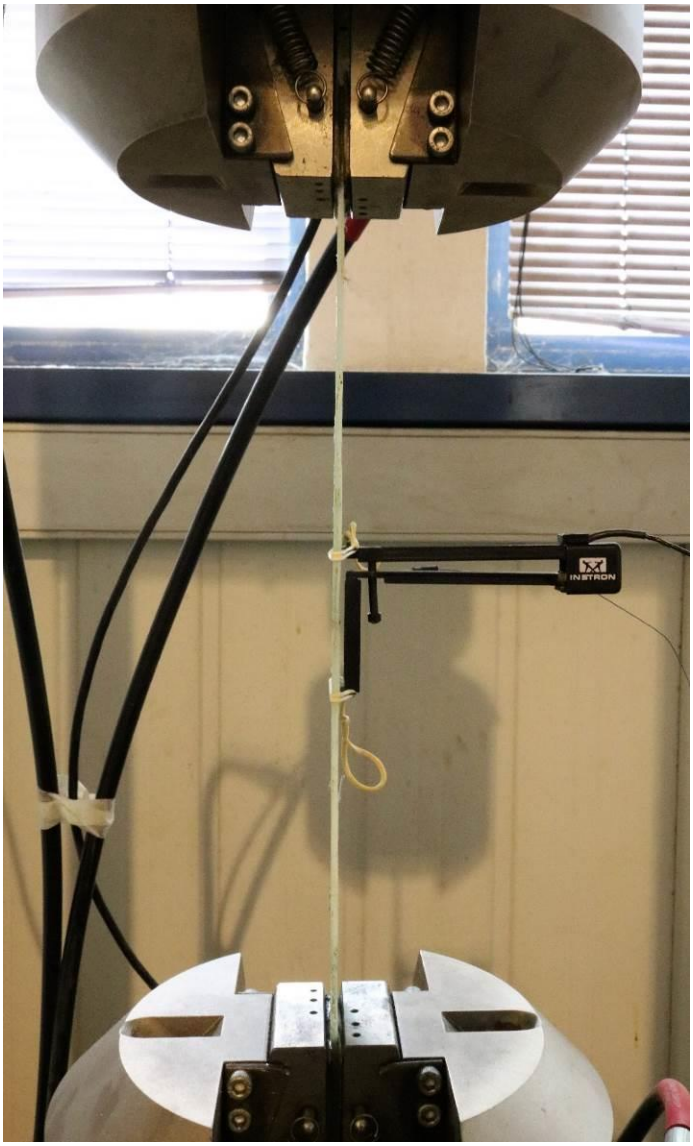

Figure 21 – Image – Tensile experimental set up

4.EXPERIMENTAL RESULTS

4.1.1 Four-point bending experiment equations

During four point bending for the calculation of the maximum constant stress for any point between load points, the following equation has been used:

$$\sigma = \frac{3PL}{4bh^2} \quad (1)$$

Where:

$\sigma =$ stress at the outer surface in the load span region, MPa
$P =$ applied force, N
$L =$ support span, mm
$b =$ specimen width, mm
$h =$ thickness of beam, mm

The maximum strain in the middle of the outer surface (at the maximum bending arrow) was calculated using the following expression:

$$\varepsilon = \frac{4.36\delta h}{L^2} \quad (2)$$

Where:

$\varepsilon =$ maximum strain at the outer surface, *mm/mm*
$\delta =$ mid-span deflection, *mm*
$L =$ support span, *mm*
$h =$ thickness of beam, *mm*

The flexural modulus of elasticity is calculated from:

$$E = \frac{0.17L^3m}{bh^3} \quad (3)$$

Where:

$E =$ flexural secant modulus of elasticity, *MPa*
$L =$ support span, *mm*
$b =$ width of beam, *mm*
$h =$ thickness of beam, *mm*
$m =$ slope of the secant of the force-deflection curve

4.1.2 Tensile experiment equations

The maximum tensile stress is calculated by means of the following equation:

$$F = \frac{Pmax}{A} \quad (4)$$

Where:

F^{tu} = ultimate tensile strength, *MPa*

P^{max} = maximum load prior to failure, *N*

A = average cross-sectional area, mm^2

The maximum tensile elongation is calculated from:

$$\varepsilon = \frac{\delta}{L} \quad (5)$$

Where:

ε = tensile strain at i-th data point , $\mu\varepsilon$

δ = extensometer displacement at i-th data point , *mm*

L = extensometer gage length, *mm*

Tensile chord modulus of elasticity is calculated by:

$$E = \frac{\Delta\sigma}{\Delta\varepsilon} \quad (6)$$

Where:

E = tensile chord modulus of elasticity, *GPa*

$\Delta\sigma$ = difference chord modulus of elasticity, *MPa*

$\Delta\varepsilon$ = difference between two strain points

4.2 Bending test results

The first test was carried out on a test specimen according to ASTM standard and a failure occurred at the contact points of the jig rollers (Figure 22) at relatively small load. This happened due to the sinking of the harder roller material into the relatively soft multilayer layout of the specimen supported by the stress concertation imposed at this point during bending. So, for the next tests, special protective pads were constructed and placed at the contact-load points to minimize the stress concertation effects (Figure 23).

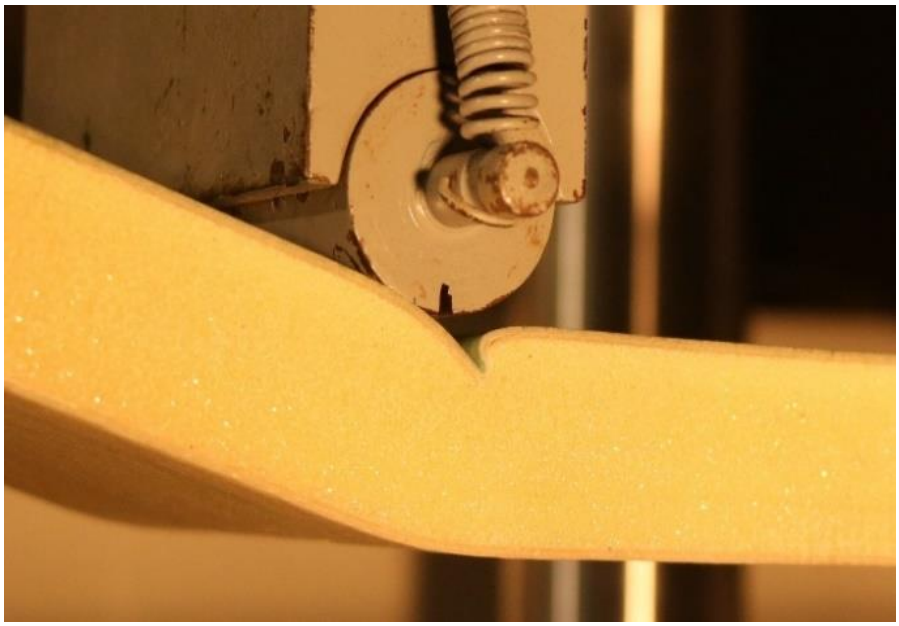

Figure 22 – Image – Failure of specimen tested without pads

Figure 23 – Image – Testing of specimen with the use of pads

During flexural loading, failures were observed in two different regions. The specimens that had 20mm and 30mm stepped overlap repair in their structures failed at the upper region where the root of the repair is found, where compressive stresses develop (Figure 24), while the specimens with 40mm stepped repair failed at the locations of contact with the protective pads.

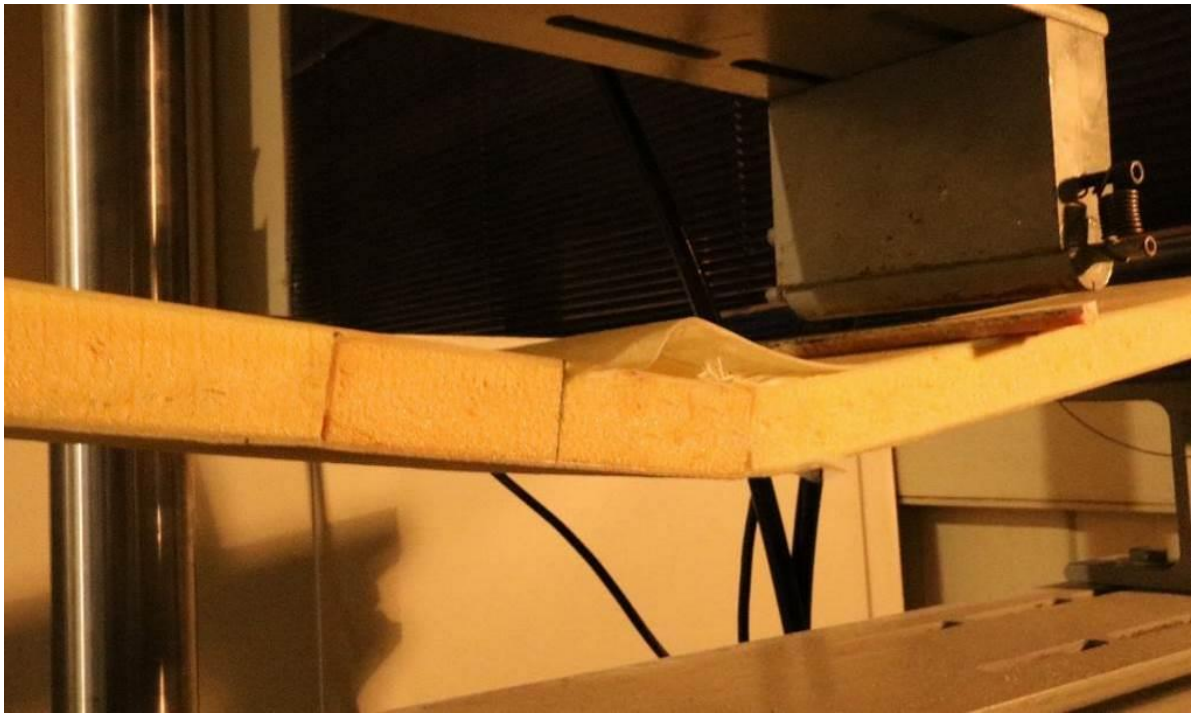

Figure 24 – Image – Failure of specimen with stepped 20mm overlap repair in the compression side

As shown in the diagrams of the performed bending tests in Figures 25,26 and taking into account the experimental scatter observed, the reference specimens exhibit lower flexural strength compared to the specimens containing the stepped repair something that is also compatible to the stiffness of the panels. Also, it is observed that with increasing the length of the step in the repair procedure, the bending strength of the specimens is increased. The increase in bending stiffness and strength of the repaired specimens is a welcome feature regarding the maintenance procedure of such structural components. The reason for this increase lies in the nature of the repair technique, which in order to fill the gap created by the removal of the composite damaged material, finally by the stepped overlap method higher density of glass-fiber plies (double fiber-fabrics in the overlap regions) is found in the repair area ,than the original undamaged configuration. This, contributes to an increased bending stiffness at the area of the repair and hence requires a higher load for failure.

In order to explain the above variation of bending stiffness, the fiber density increased in the repaired specimens was estimated according to the following formula and the results are shown in Table 5. It has to be commented that, the fiber density increases due to the overlaps, shown in the following table, is distributed only close to the repair region (inside the loading span), which results in an important increase of flexural stiffness.

$$Total\ triaxial\ overlap\ length = number\ of\ the\ triaxial\ layers \times overlap\ length\ \times 2\ sides \quad (\mathbf{1})$$

$$Total\ biaxial\ overlap\ length = number\ of\ the\ biaxial\ layers \times overlap\ length\ \times 2\ sides \quad (\mathbf{2})$$

$$Excesive\ fiber\ wheight\ caused\ by\ the\ repair = \left[(\mathbf{1}) \times 1185\,\frac{g}{m^2} + (\mathbf{2}) \times 310\,\frac{g}{m^2}\right] \times specimen\ width\ (\mathbf{3})$$

	Biaxial overlap length (mm)	Triaxial ovelap length (mm)	Specimen width (mm)	Total excesive fiber weight (gr)	Final total fiber phase weight (gr)	Diefferentiation percentage
No repair	-	-	120	-	433.2	-
20mm overlap	160	80	120	17.328	450.528	4%
30mm overlap	240	120	120	25.992	459.192	6%
40mm overlap	320	160	120	34.656	467.856	8%

Table 5 – Excessive weight of the fibrous phase cause by the repair overlaps

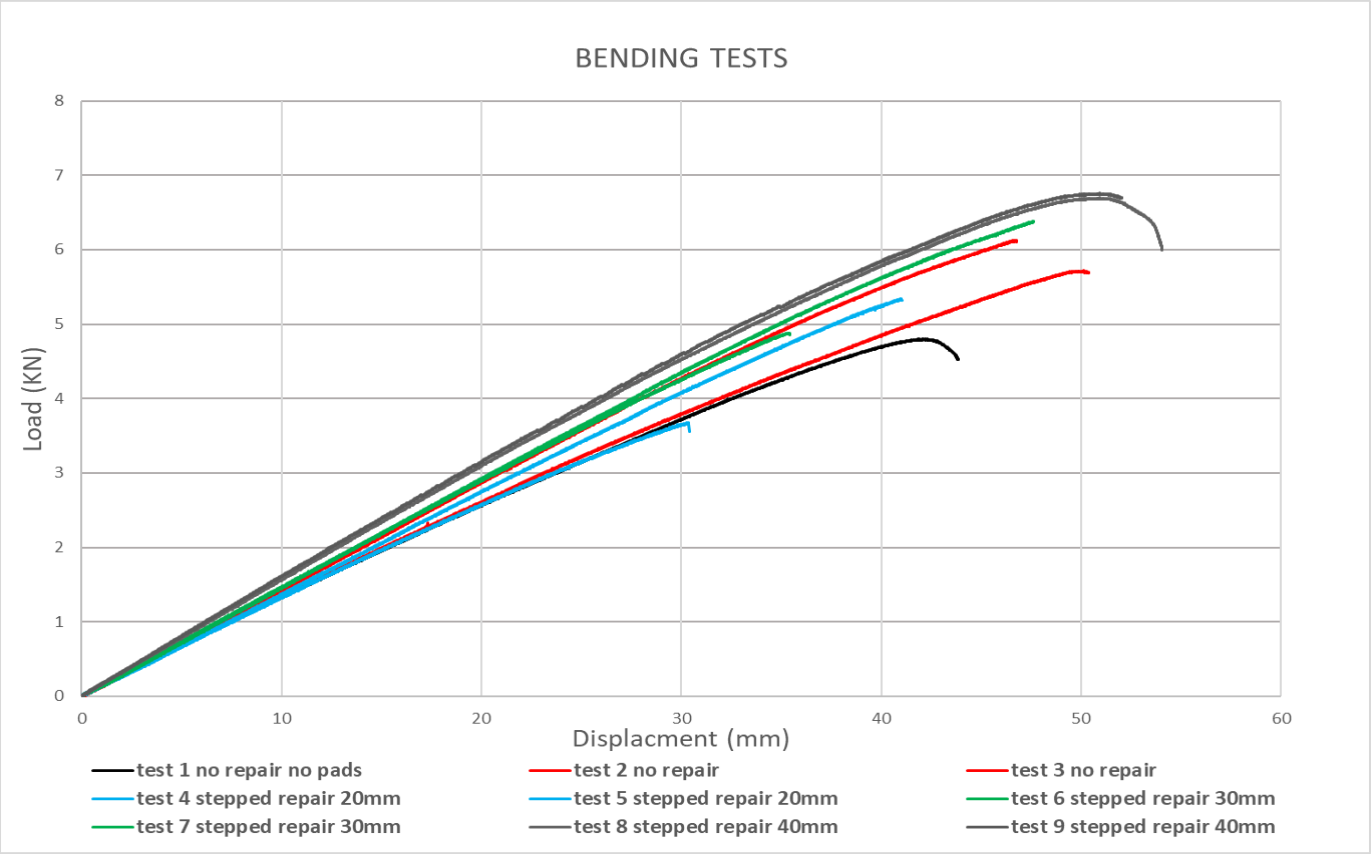

Figure 25 – Diagram – Load-Displacement

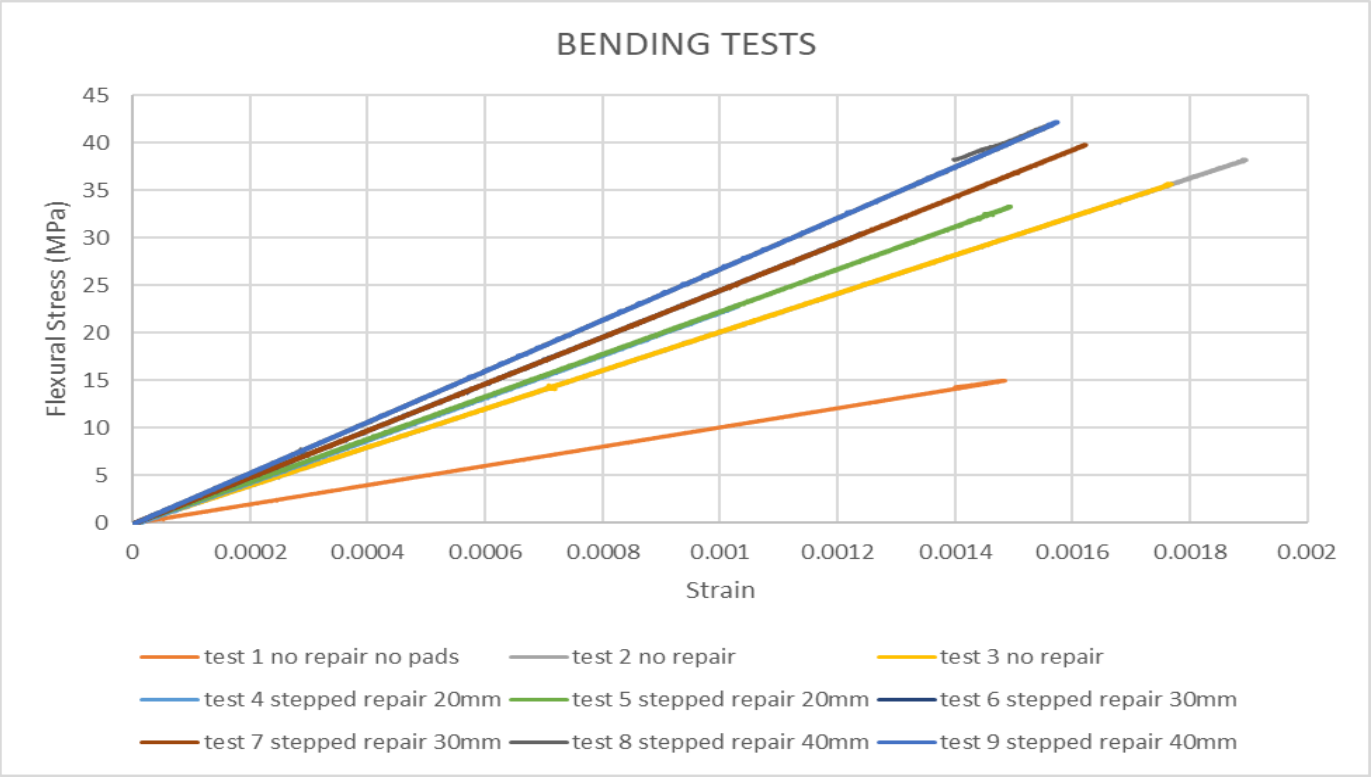

Figure 26 – Diagram – Stress - Strain

Test	Specimen	Max load (Kn)	Extension (mm) @max load	Average load (Kn)	Max flexural stress (MPa)	Average Stress (Mpa)	Strain @max stress	Bending modulus of elasticity (GPa)	Failure code
1	No repair no pads	4.8067	42.9681	-	15.0209		0.001485		CAL
2	No repair	6.1286	46.7040	5.9237	38.3039	37.0237	0.001895	19.96	SBV
3	No repair	5.7189	50.1310		35.7435		0.001769		SBV
4	Step 20mm	3.6784	30.3211	4.51	23.0062	28.1957	0.001026	22.07	CBM
5	Step 20mm	5.3416	41.0181		33.3852		0.001494		CBM
6	Step 30mm	4.8797	35.3436	5.6312	30.4982	35.1953	0.001240	24.28	CBM
7	Step 30mm	6.3827	47.5886		39.8924		0.001623		CBM
8	Step 40mm	6.6981	50.9520	6.7284	41.8631	42.0530	0.001560	26.50	CAL
9	Step 40mm	6.7588	51.0230		42.2430		0.001570		CAL

Table 6 – Four-point bending experiment results

Failure codes:

- **CAL** = Failure at the compression side at the left loading nose
- **SBV** = Interlaminar shear failure between the loading noses in various locations
- **CBM** = Failure at the compression side in the middle area between the loading noses

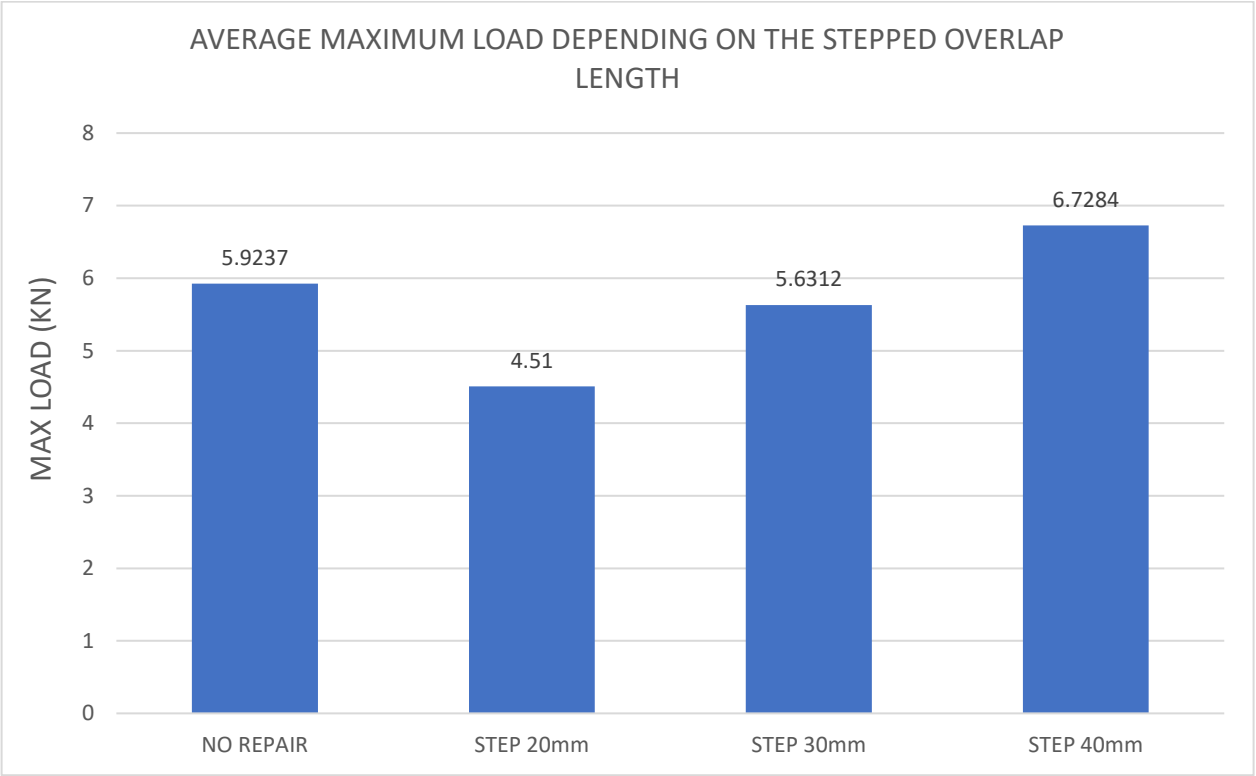

Figure 27 – Diagram – Comparison of the maximum load between every category of specimens

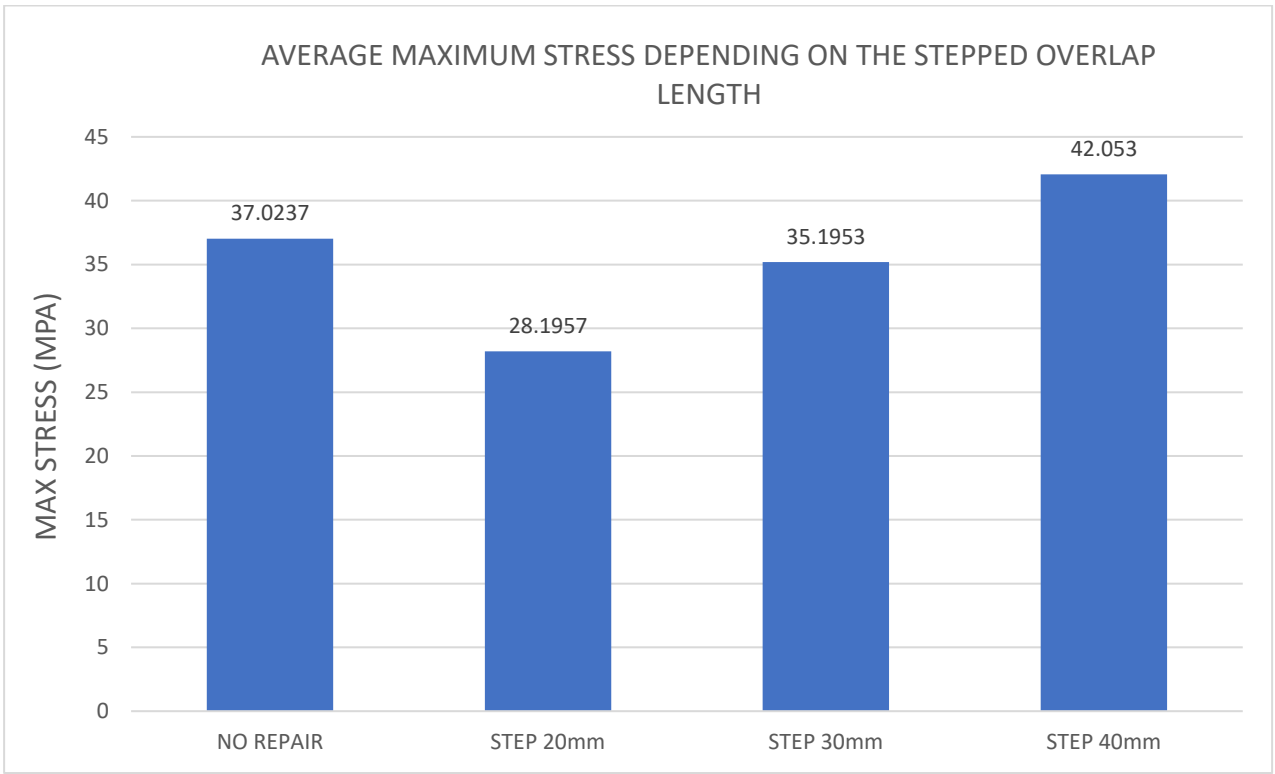

Figure 28 – Diagram – Comparison of the maximum stress between every category of specimens

4.3 Tensile experiment

The ASTM standard proposed the construction of protective pads and their attachment to the ends of the specimens to avoid failures at the points where the grippers and the specimens catch, so after 20 tests no failure of the grippers occurred. In Figure 29 it is shown how the protective pads act as a shield to the main fibrous phase of the tensile specimen.

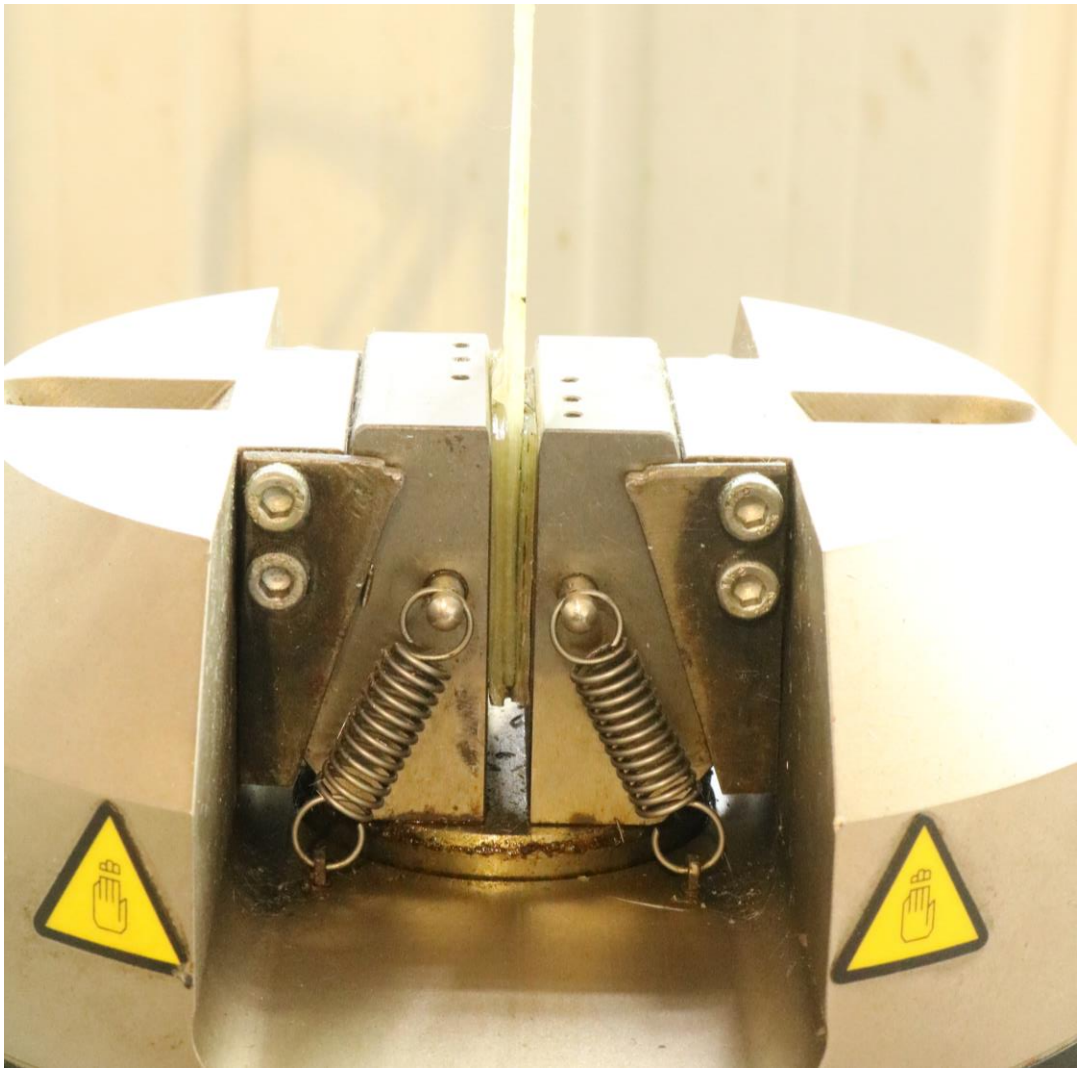

Figure 29 – Image – Protective pads compressed by the grippers

In Figures 30 through 37 the stress-strain and load-displacement diagrams, such as concentrated Tables are shown for every tensile experiment separately. Finally, comparative Figures 38,39,40,41,42 were created, in order to give us the ability to easily compare the mechanical behavior between the reference specimens (no repair) and the other three types of repaired specimens.

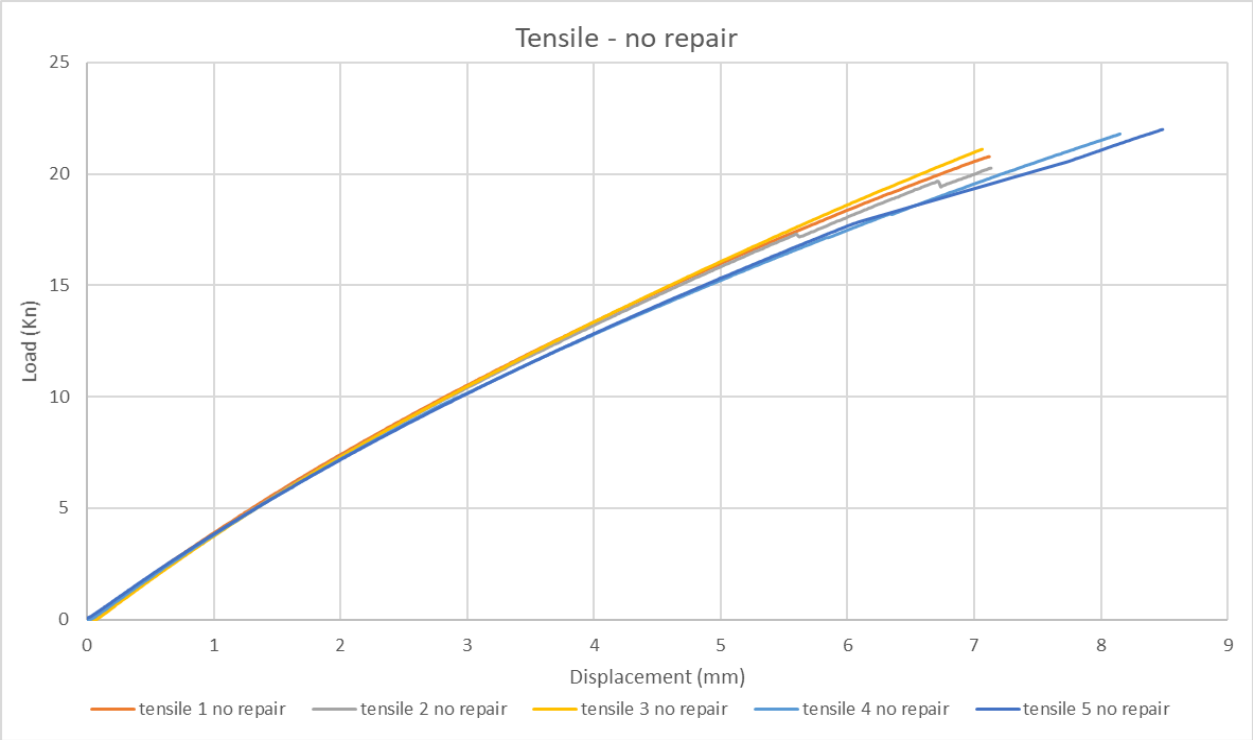

Figure 30 – Diagram – Load-displacement curve of tensile specimen without repair

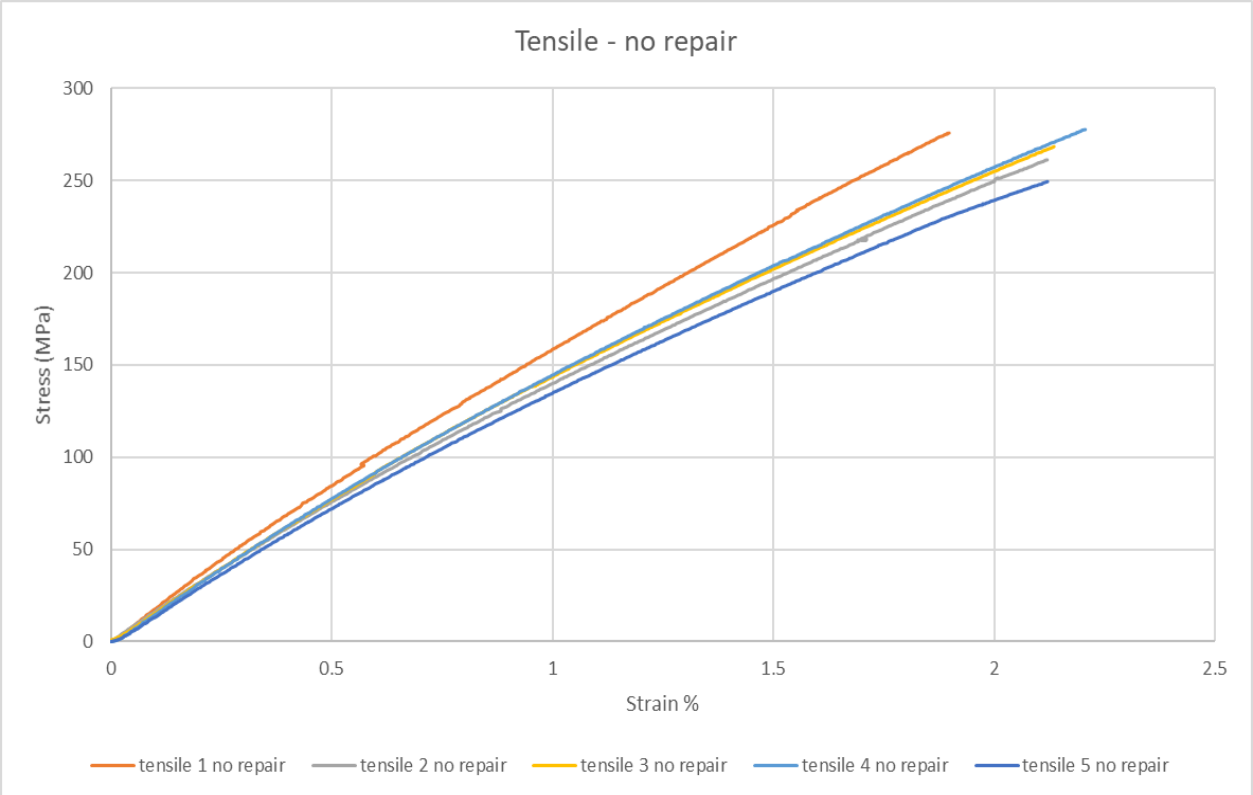

Figure 31 – Diagram – Stress-strain curve of test specimen without repair to its structure

Test	Max load (Kn)	Extension (mm) @max load	Max stress (MPa)	Max strain @max load	Tensile Chord modulus (GPa)	Average max load (Kn)	Average max stress (MPa)	Average tensile Chord modulus (GPa)	Failure code
Tensile 1 no repair	20.7767	7.1182	288.1887	1.9407	17.99	21.1874	276.3350	15.998	XGM
Tensile 2 no repair	20.2604	7.1318	262.4816	2.6358	15.95				XGM
Tensile 3 no repair	21.1100	7.0625	268.4074	2.1928	15.90				XGM
Tensile 4 no repair	21.7931	8.1491	277.6552	2.6710	15.72				XGB
Tensile 5 no repair	21.9971	8.4854	284.9422	2.1206	14.43				XGB

Table 7 – Tensile experiment results of specimens with no repair in their structure

Failure codes:

- **XGM** = Explosive failure in the middle of the gage length
- **XGB** = Explosive failure in the bottom part of the gage length

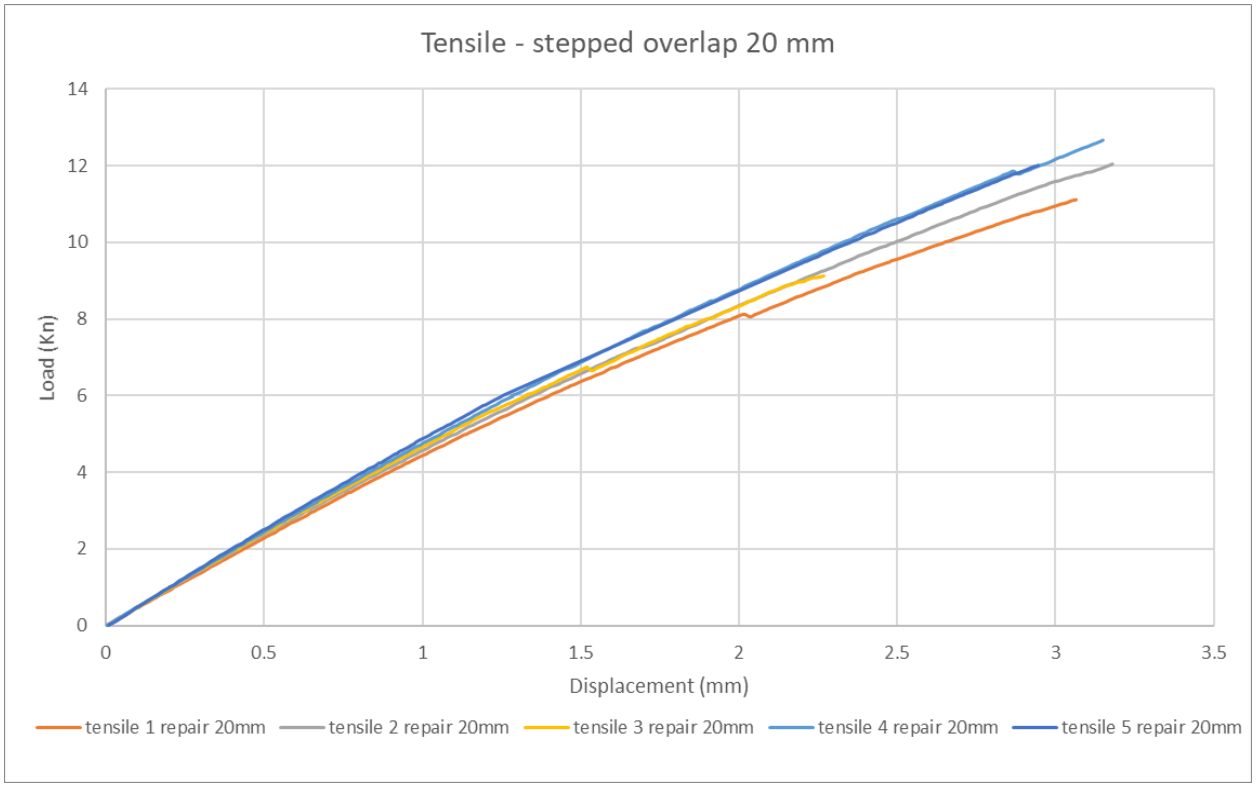

Figure 32 – Diagram – Load-Displacement curve of test specimen with 20mm overlap repair to its structure

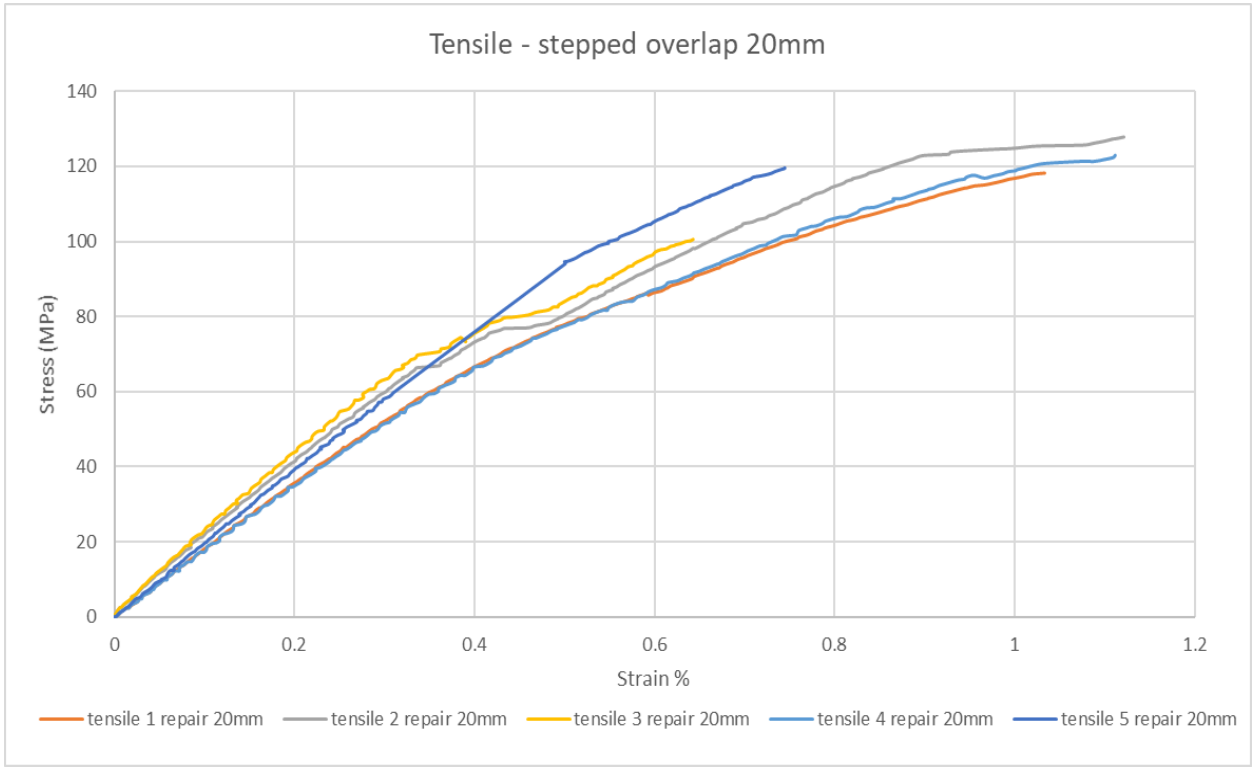

Figure 33 – Diagram – Stress-strain curve of test specimen without 20mm overlap repair to its structure

Test	Max load (Kn)	Extension (mm) @max load	Max stress (MPa)	Max strain @max stress	Tensile Chord modulus (GPa)	Average max load (Kn)	Average max stress (MPa)	Average tensile Chord modulus (GPa)	Failure code
Tensile 1 stepped repair 20mm	11.1125	3.0654	118.2170	1.0334	17.8	11.5396	119.0078	19.68	MGM
Tensile 2 stepped repair 20mm	12.0425	3.1802	127.8367	1.1214	20.67				MGM
Tensile 3 stepped repair 20mm	9.1242	2.2680	100.5748	0.64	19.16				MGM
Tensile 4 stepped repair 20mm	12.6657	3.1504	125.6587	1.2140	17.41				MGM
Tensile 5 stepped repair 20mm	12.7531	2.9456	122.7521	0.9546	23.38				MGM

Table 6 – Tensile experiment results of specimens with 20mm overlap repair in their structure

Failure codes:

- **MGM** = Multimode failure in the middle of the gage length

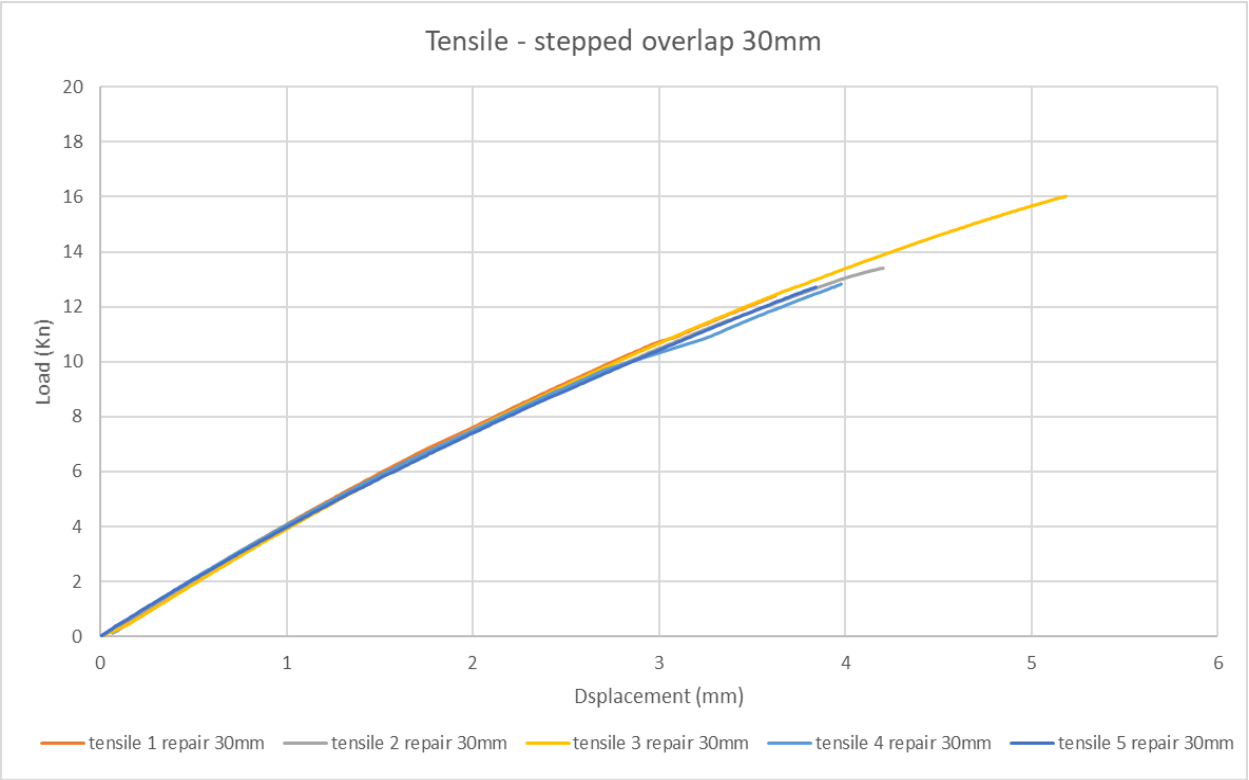

Figure 34 – Diagram – Load-Displacement curve of test specimen with 30mm overlap repair to its structure

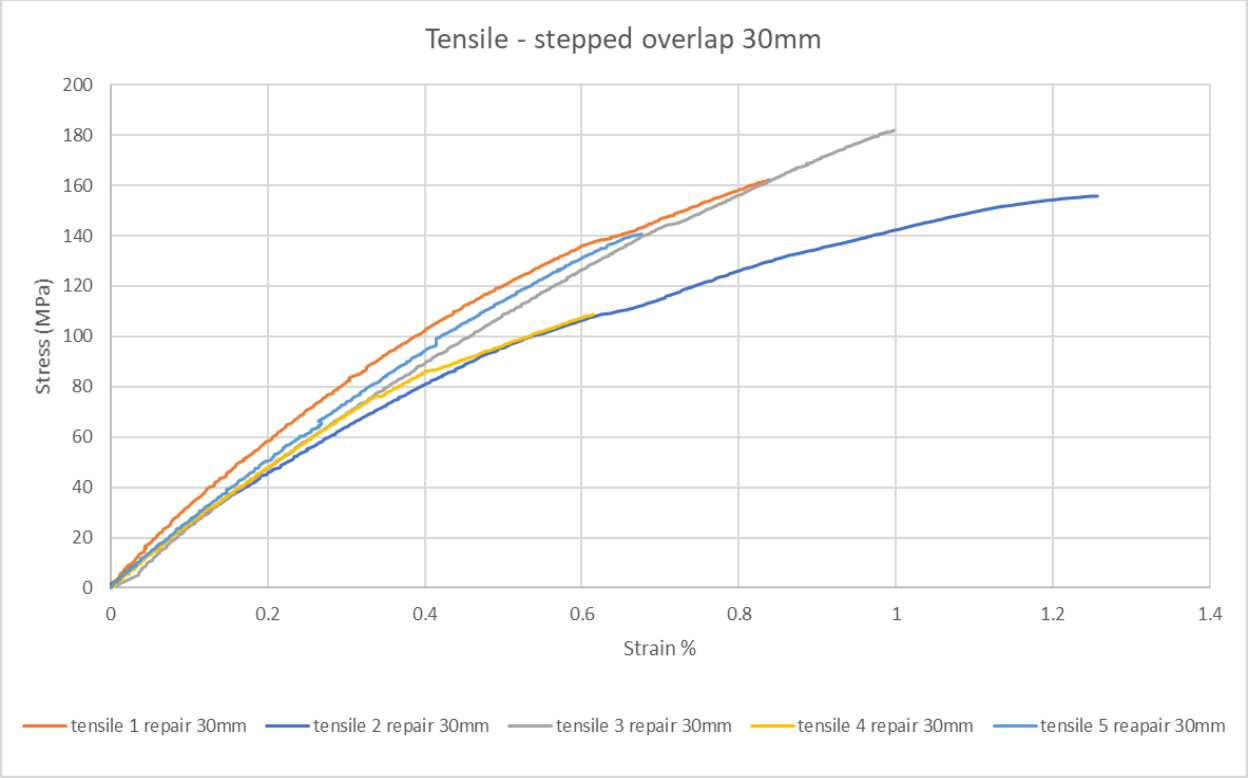

Figure 35 – Diagram – Stress-strain curve of test specimen with 30mm overlap repair to its structure

Test	Max load (Kn)	Extension @max load	Max stress (MPa)	Max strain @max stress	Tensile Chord modulus (GPa)	Average load (Kn)	Average stress (MPa)	Average tensile Chord modulus (GPa)	Failure code
Tensile 1 stepped repair 30mm	12.3977	3.6235	162.2047	0.8392	29.18	13.4751	149.8798	24.79	MGM
Tensile 2 stepped repair 30mm	13.3999	4.1389	155.7787	1.2561	22.30				MGM
Tensile 3 stepped repair 30mm	16.0262	5.1843	181.8984	0.9971	23.68				MGM
Tensile 4 stepped repair 30mm	12.8323	3.9777	108.8362	0.6149	23.90				MGM
Tensile 5 stepped repair 30mm	12.7195	3.8414	140.6810	0.6760	24.92				MGM

Table 8 – Tensile experiment results of specimens with 30mm overlap repair in their structure

Failure codes:

- **MGM** = Multimode failure in the middle of the gage length

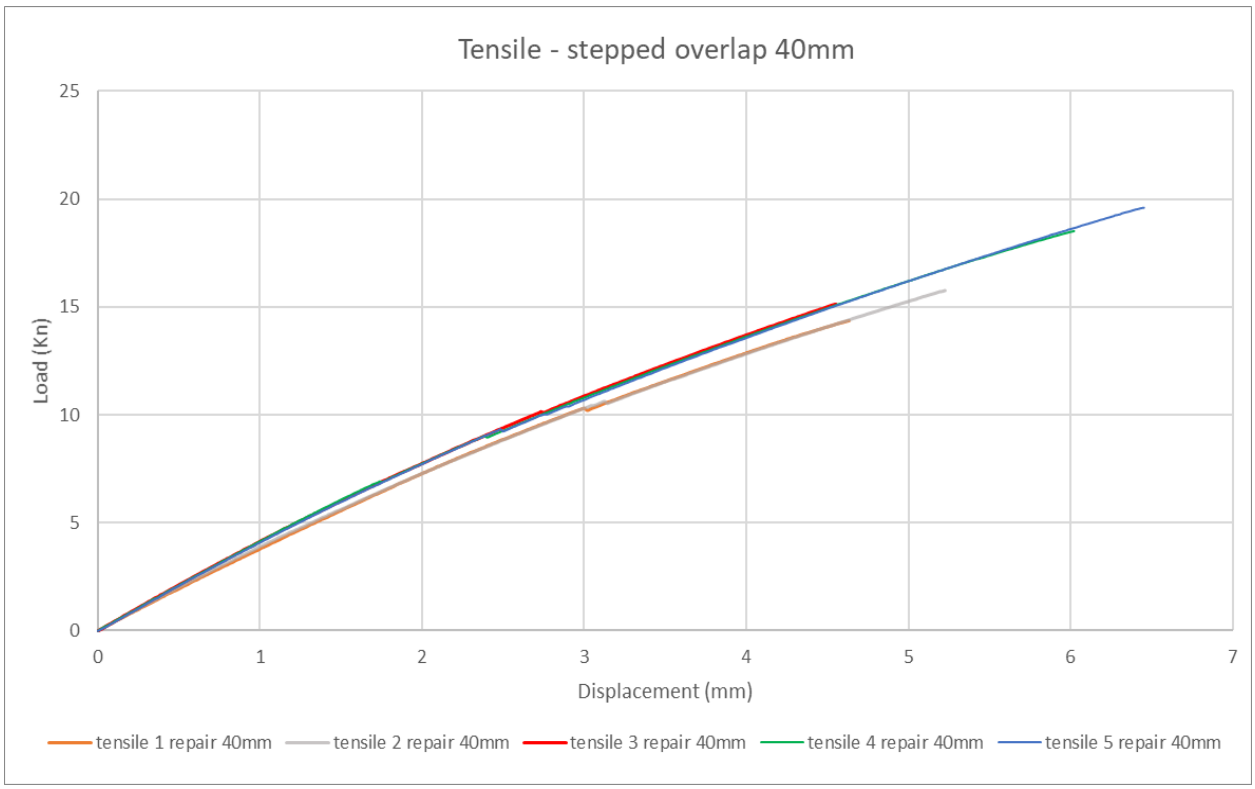

Figure 36 – Diagram – Load-Displacement curve of test specimen with 40mm overlap repair to its structure

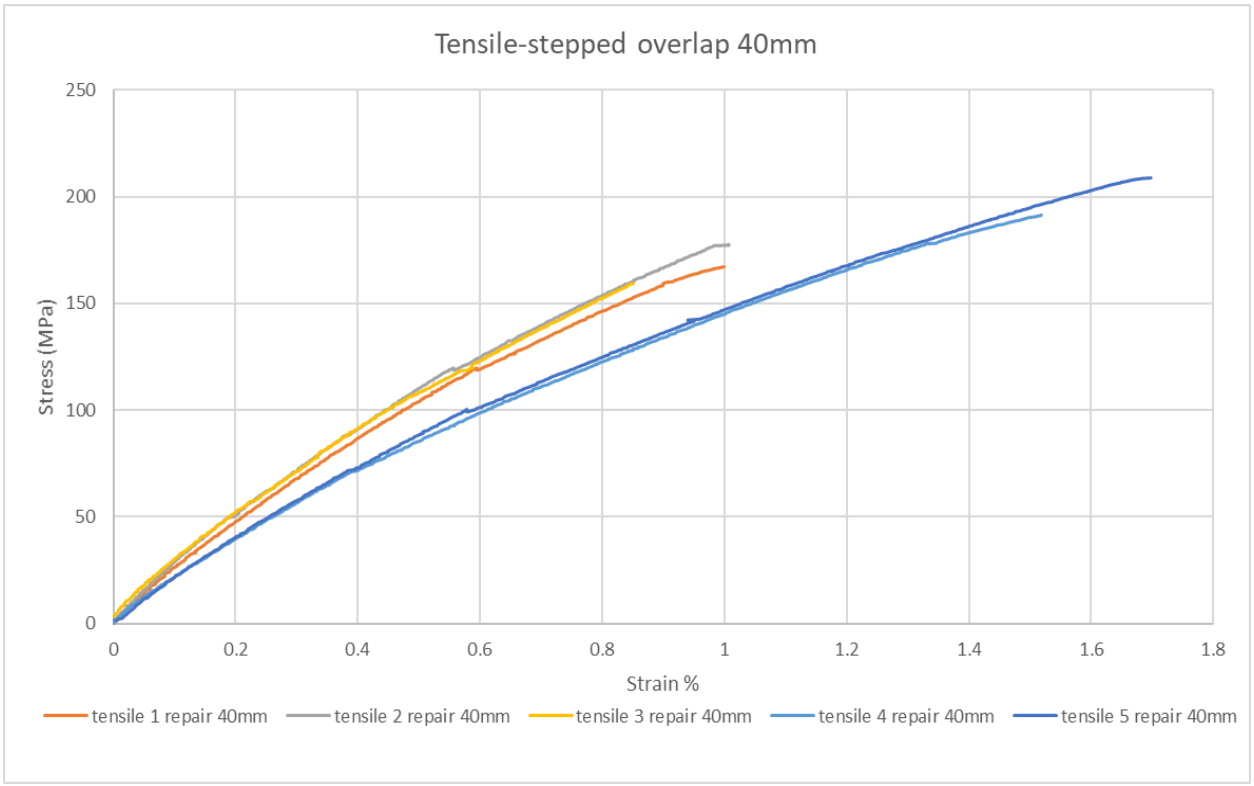

Figure 37 – Diagram – Stress - Strain curve of test specimen with 40mm overlap repair to its structure

Test	Max load (Kn)	Extension @max load	Max stress (MPa)	Max strain @max stress	Tensile Chord modulus (GPa)	Average max load (Kn)	Average max stress (MPa)	Average tensile Chord modulus (GPa)	Failure code
Tensile 1 stepped repair 40mm	14.3630	4.6341	180.2582	0.9993	23.97	16.8404	183.4984	23.46	MGM
Tensile 2 stepped repair 40mm	16.5929	5.2257	177.6393	1.0072	26.04				MGM
Tensile 3 stepped repair 40mm	15.1361	4.5517	159.4004	0.8504	26.49				MGM
Tensile 4 stepped repair 40mm	18.5149	6.0210	191.3703	1.5186	20.10				MGM
Tensile 5 stepped repair 40mm	19.5954	6.4519	208.8279	1.6978	20.70				MGM

Table 9 – Tensile experiment results of specimens with 30mm overlap repair in their structure

Failure codes:

- **MGM** = Multimode failure in the middle of the gage length

In the following Figures comparison of the “strongest” specimens of each category is made:

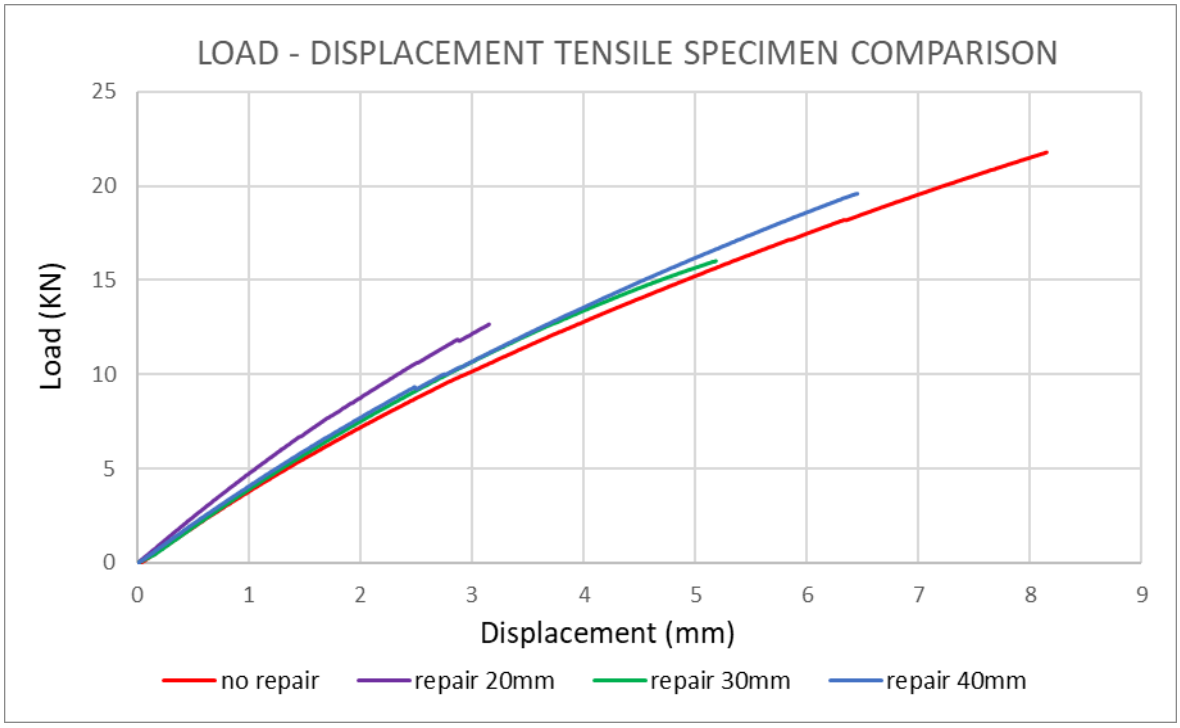

Figure 38 – Diagram – Load -Displacement comparison curve of all specimen categories

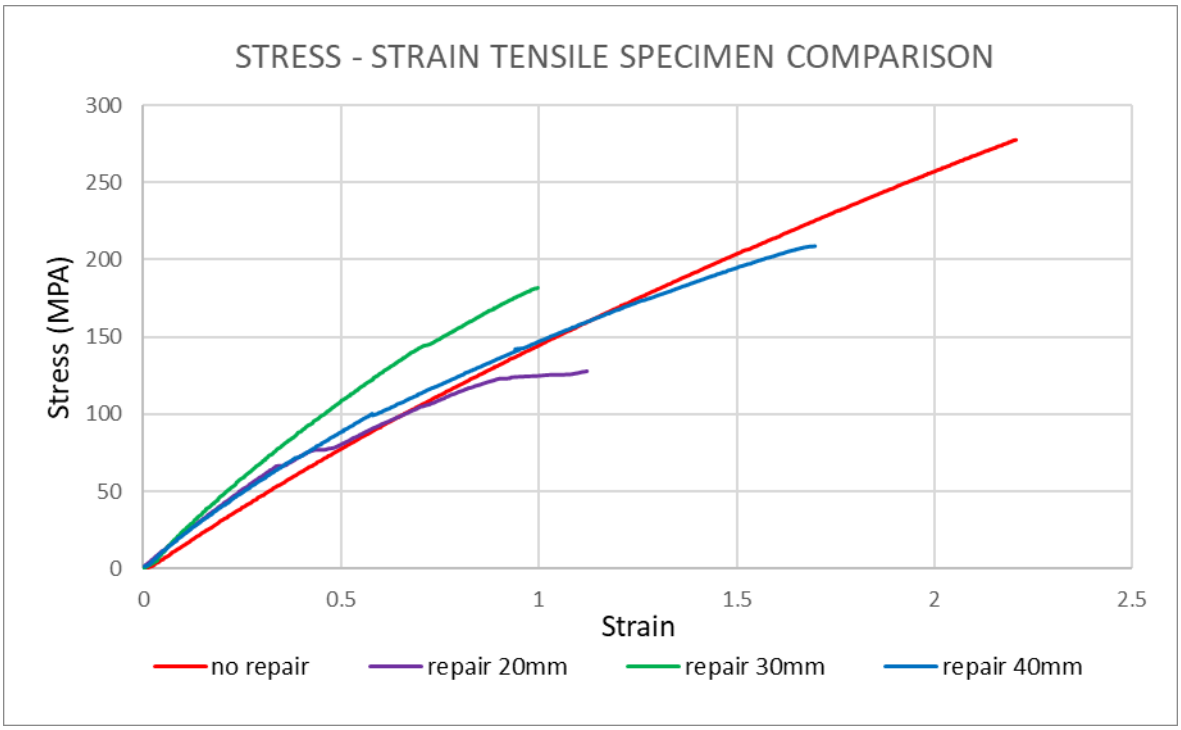

Figure 39 – Diagram – Stress - Strain curve comparison of all specimen categories

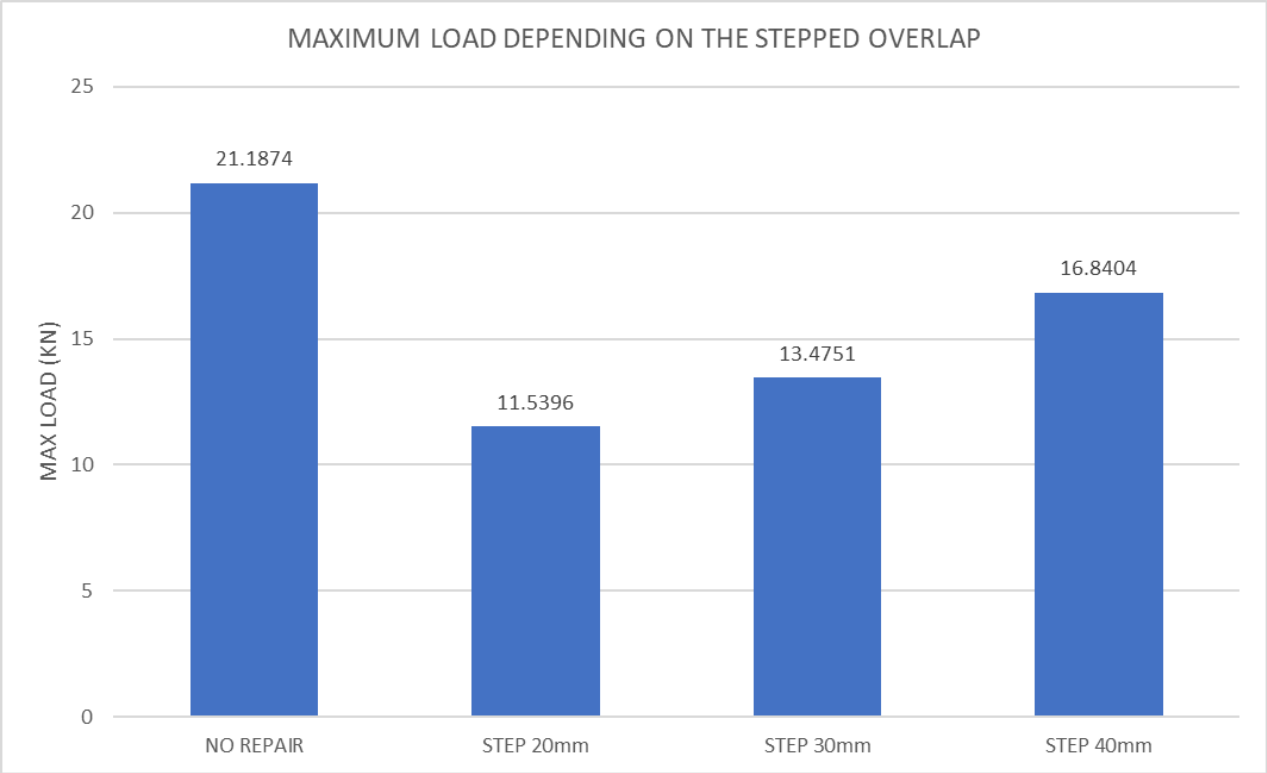

Figure 40 – Diagram – Comparison of the maximum load between every category of tensile specimens

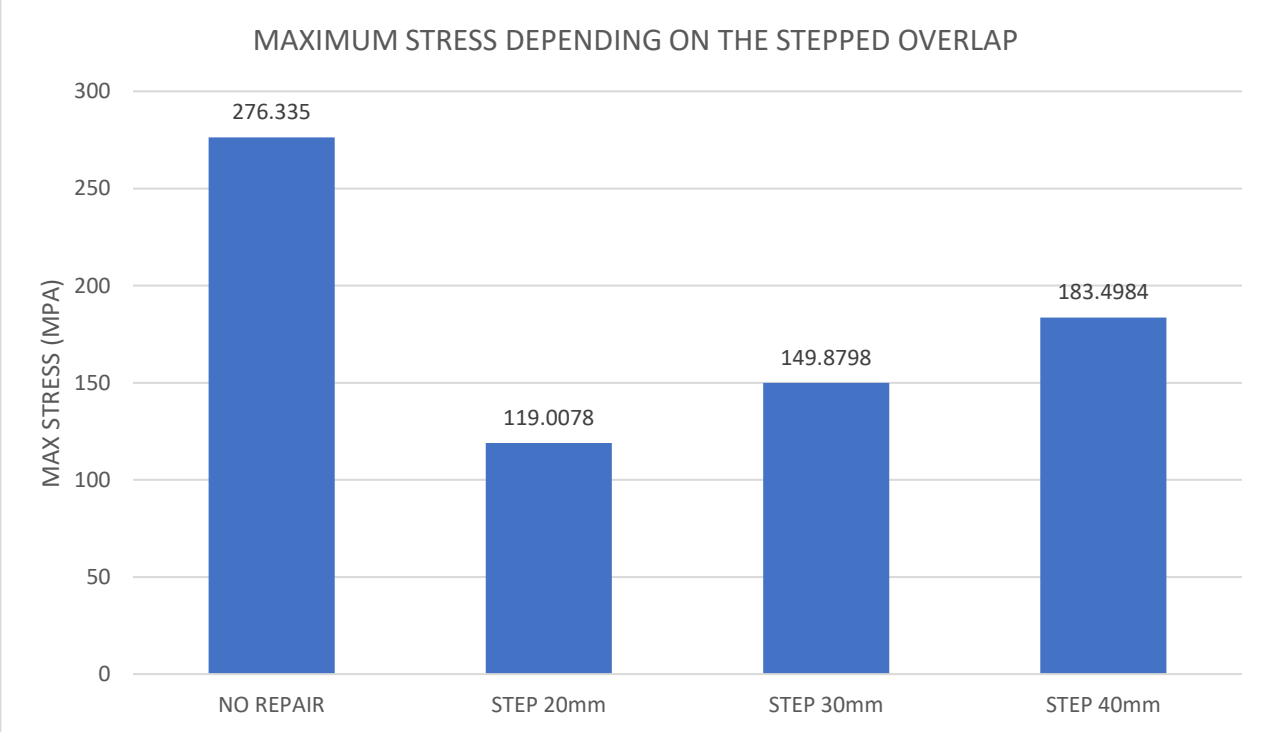

Figure 41 – Diagram – Comparison of the maximum stress between every category of tensile specimens

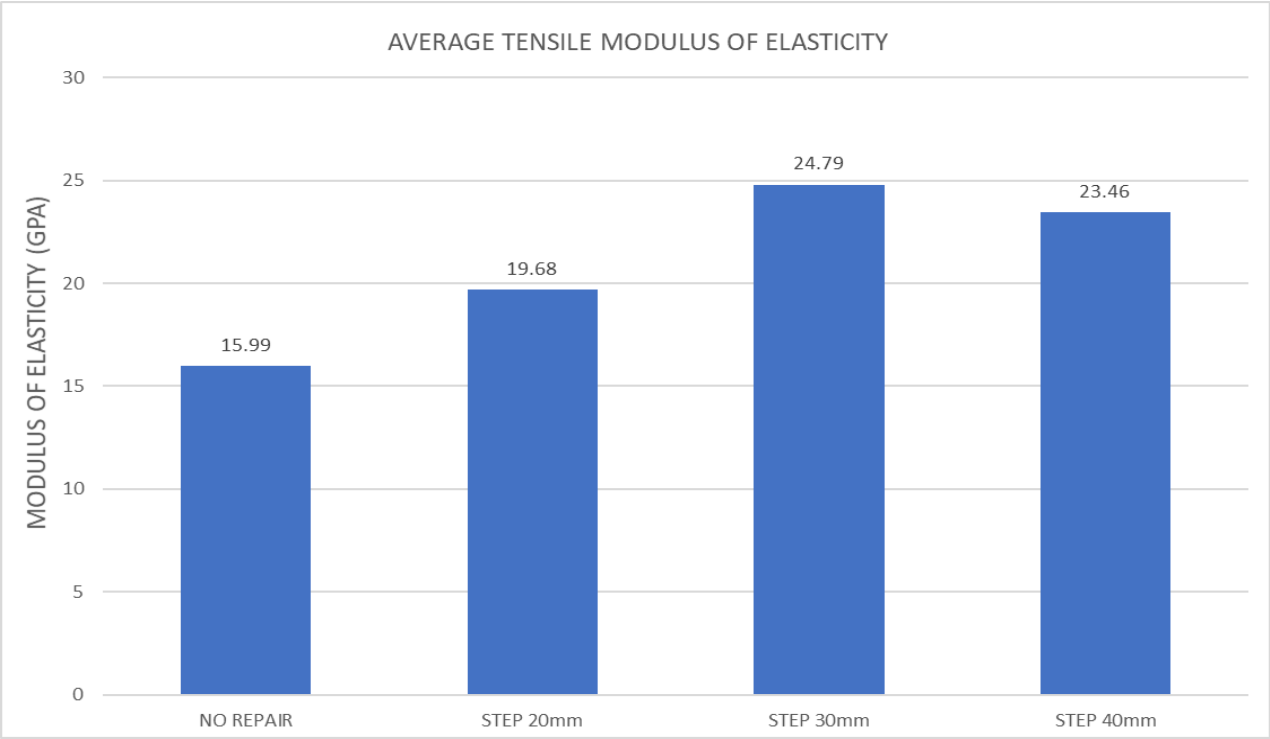

Figure 42 – Diagram – Average tensile modulus of elasticity

4.4 Fracture analysis

During the experimental the fracture patterns of the specimens have been investigated in order to understand better the failure mechanism by analyzing the failed (destroyed, cracked) lamination layout. From this analysis we are able to draw conclusions about the failure sequence and by this to understand which is the weakest point of a repaired composite sandwich structure.

4.4.1 Four-point bending specimen fracture analysis

In repaired composite specimens, fracture during bending, in the most cases occurred at the upper side of the beam (specimen), where compression takes place, at the locations close to the edge of the repair steps, which due to the discontinuity imposed in the laminate structure by the repair and following the adhesion of new glass fiber layers, impose certain stress concertation at the specific point, as well as a non-uniform stiffness and hence stress distribution at the specific area. This leads to the fracture initiation at this area of the compressive side, which is followed by delamination failure. Damage evolution in the final stage is cracking at the upper part of the laminate, this sequence is shown in Figure 43.

Figure 43 – Image – Four-point bending specimen with stepped repair in its structure – Delamination failure mechanism and fiber breakage

Specimens without a repair in their structure have continuous fibrous phase which means that the stresses are evenly distributed without high stress concertation in any certain areas. The failure mechanism is characterized as delamination of the outer lamination on the compressive side, which is followed by cracking of the core material as shown in Figure 44. The delamination is result of the differentiation of stresses between the two sides, compression in the upper side tension in the lower side.

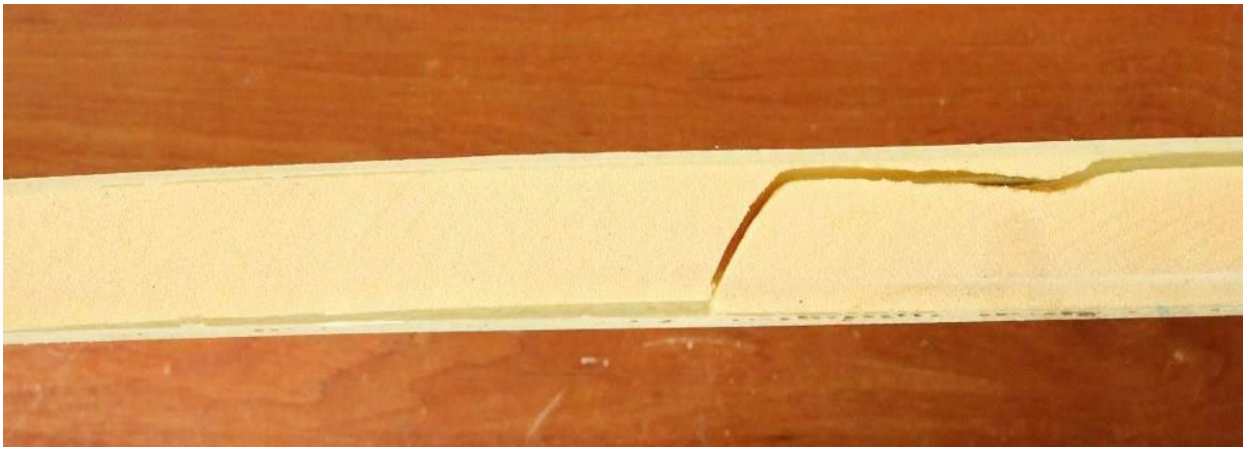

Figure 44 – Image – Four-point bending specimen without repair in its structure- Delamination failure mechanism

4.4.2 Tensile specimen fracture

All tensile specimens with repair in their structure showed almost the same failure pattern shown in Figure 45. Firstly, a delamination starts from the root of the repair where there is the triaxial fiber fabric. When the total delamination between the triaxial fiber fabrics happens, the redistribution of stresses leads to high concentration of stresses only on the two biaxial fabrics. These fabrics are well joined together and the fibers have different direction than the direction of the tensile forces, these parameters act as barrier to the delamination mechanism, which results to the total breakage of the two biaxial fiberglass layers.

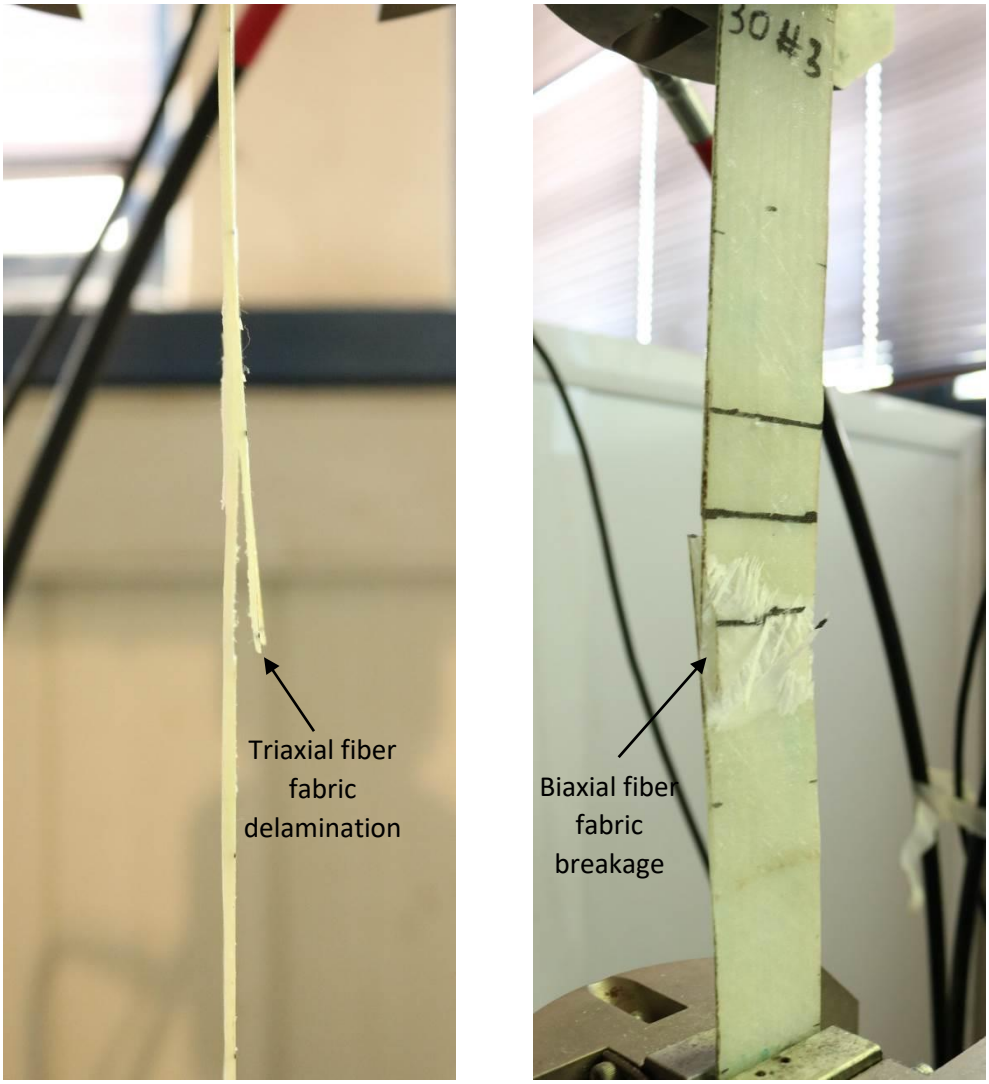

Figure 45 – Image – Tensile specimen with stepped repair in its structure – Delamination and fiber breakage

The tensile specimens without repair in their structure exhibited higher durability under tension in comparison to the specimens with repair in their structure. The elongation and the forces that these specimens can handle is much higher than the specimens with repair. By having continuous fiber phase, and evenly distrusted stresses the failure-delamination mechanism has no place to start. The glass fibers can withstand high elongation something that happens in this series of experiments, but the matrix material which has high stiffness cannot elongate as much and eventually of the above lead to the cracking of the matrix material. During the matrix failure, many small and sharp pieces are formed which are found between the stressed fibers, these small pieces and the higher stress distribution only in the fibrous phase eventually lead to fiber breakage as it is shown in Figure 46.

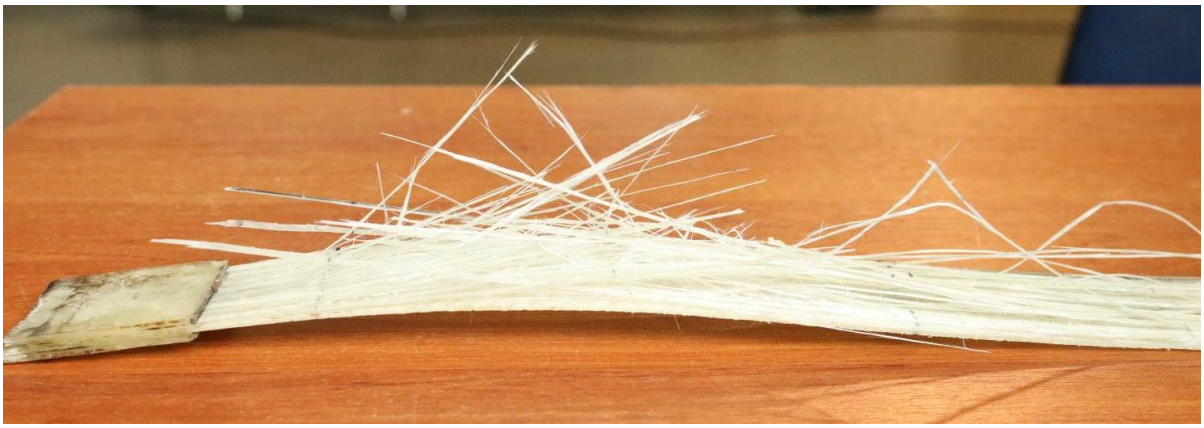

Figure 46 – Image –Tensile specimen with no repair in its structure – Matrix and fiber failure

In Figure 47 a comparison between the failure modes in different categories of specimens is made. It is obvious that the repaired specimen's failure is attributed to delamination and the failure in non-repaired specimens is attributed to the failure of the matrix materials.

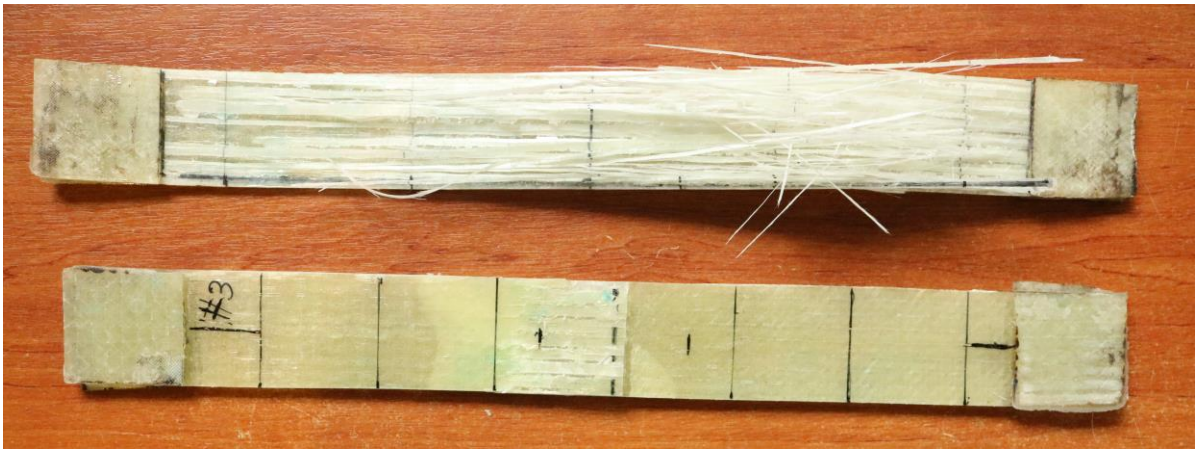

Figure 47– Image – Repaired and non-repaired Tensile specimens after failure

5. CONCLUSIONS

From the experimental investigation performed on repaired fiber reinforced composite components related to the wind turbine blade structure, important conclusions have been drawn regarding the mechanical behavior of a repaired component. One of the most important parameters of the repair procedure is the stepped overlap length in a repair region. From the above diagrams it is made clear that as the length of the overlap increases, the flexural behavior of the specimens is improved. More specifically, with the increase of overlap, the bending stiffness of the specimens increases, which means that for similar or higher loads the test specimen structure becomes less distorted. The highest mechanical properties were obtained from specimens with a stepped repair in their structure with a 40 mm overlap length. With decreasing repair length stress concentrations close to the root of the repair become more pronounced promoting failure at the compressive side at the root location.

Under uniaxial tensile loading, in contrast to the behavior observed during bending, the test specimens with no repair showed superior mechanical performance in comparison to the repaired ones. In the case of specimens with no repair in their structure, at high stresses firstly the matrix material failed which then resulted to the total destruction of the fibers. In the case of the repaired specimens the stress concentration imposed at the root of repair under tension stresses influences the composite material behavior by promoting a delamination, which is subsequently followed by breakage of fibers. Increasing the length of overlap repair leads to an increase in tensile strength, as a result of spreading the induced stress concentration, however even in the case of 40 mm overlap repair length the strength is inferior to the undamaged tension specimen.

The results obtained in the current Diploma Thesis are useful for the optimization of maintenance procedures applied in damaged outer shell of wind turbine blades. More over in the future it would be very useful if the scientific community studies and compared different types of repair and all the parameters that affect them, in order to end up with the best repair method and therefore the wind turbine technicians, will do more reliable and viable repairs.

6. BIBLIOGRAPHY

[1] Zonghong Xie, Xiang Li, Qun Yan, Scarf Repair of Composite Laminates, MATEC Web of Conferences 61,2016

[2] C. H. Wang, V. Venugopal and L. Peng, Stepped Flush Repairs for Primary Composite Structures, The Journal of Adhesion, 91:95–112, 2015

[3] History of wind turbines, Available: http://xndrmstrre64ad.dk/wpcontent/wind/miller/windpower%20web/en/pictures/brush,2017

[4] K. B. Katnam, A. J. Comer, D. Roy, L. F. M. da Silva, and T. M. Young, Composite Repair in Wind Turbine Blades: An Overview, The Journal of Adhesion, 91:113–139,2015

[5] Zafar, Syed Shahrukh, "Study of composite wind turbine spars", Theses and Dissertations, Paper 1685, Lehigh University, 2013

[6] Leon Mishnaevsky Jr., Kim Branner, Helga Nørgaard Petersen, Justine Beauson, Malcolm McGugan, Bent F. Sørensen, Materials for Wind Turbine Blades: An Overview,2017

[7] Hossein Rahmani, S. Heydar Mahmoudi, Alireza Ashori, Mahdi Golriz, Elastic Properties of Carbon Fiber Reinforced Epoxy Composites, Iranian Research Organization for Science and Technology ,2015

[8] Chun H.Wang , Cong N.Duong , Bonded Joints and Repairs to Composite Airframe Structures,2016

[9] Burton T., Sharpe D., Jenkins N. and Bossanyi E., “Wind Energy Handbook”, Wiley, USA (1991).

[10] Σαββάκη Ε.Κ. Θεοτόκογλου Ε.Ε. Διερεύνηση διαφορετικών ινοπλισμένων σύνθετων υλικών πτερυγίου ανεμογεννήτριας και συμπεριφορά του σε λογισμό λόγω κάμψης Μεταπτυχιακή Εργασία Δ.Π.Μ.Σ.: Εφαρμοσμένη Μηχανική, Εθνικό Μετσόβιο Πολυτεχνείο, Αθήνα, 2015.

[11] ASTM D 7264/D 7264M-07 Standard Test Method for Flexural Properties of Polymer Matrix Composite Materials

[12] ASTM D 3039/D3 039M-95a Standard Test Method for Tensile Properties of Polymer Matrix Composite Materials